Journal Pre-proof

Ceramisation of hazardous elements: benefits and pitfalls of the inertisation through silicate ceramics

Matteo Ardit, Chiara Zanelli, Sonia Conte, Chiara Molinari, Giuseppe Cruciani, Michele Dondi

This is a PDF file of an article that has undergone enhancements after acceptance, such as the addition of a cover page and metadata, and formatting for readability, but it is not yet the definitive version of record. This version will undergo additional copyediting, typesetting and review before it is published in its final form, but we are providing this version to give early visibility of the article. Please note that, during the production process, errors may be discovered which could affect the content, and all legal disclaimers that apply to the journal pertain.

Ceramisation of hazardous elements: benefits and pitfalls of the inertisation through silicate ceramics

Matteo Ardit[1], Chiara Zanelli[2], Sonia Conte[2*], Chiara Molinari[2], Giuseppe Cruciani[1], Michele Dondi[2]

[1]Physics and Earth Sciences Department, University of Ferrara, Via Saragat 1, 44122 Ferrara, Italy

[2]CNR–ISTEC, Institute of Science and Technology for Ceramics, Via Granarolo 64, 48018 Faenza, Italy

Corresponding author: Sonia Conte, sonia.conte@istec.cnr.it

Address: CNR–ISTEC, Via Granarolo 64, 48018 Faenza (Italy)

Abstract

The addition of wastes to silicate ceramics can considerably expand the compositional spectrum of raw materials with a possible inclusion of hazardous components. The present work quantitatively examines relevant literature to determine whether the benefits of incorporating hazardous elements (HEs) into silicate ceramics outweigh the pitfalls. The mobility of various HEs (Ba, Zn, Cu, Cr, Mo, As, Pb, Ni, and Cd) has been parameterised by three descriptors (immobilisation efficiency, mobilised fraction, and hazard quotient) using leaching data. HEs can be incorporated into both crystalline and glassy phases, depending on the ceramic body type. Moreover, silicate ceramics exhibit a remarkably high immobilisation efficiency (often exceeding 99.9%), as accomplished for Ba, Cd, Ni, and Zn elements. The pitfalls of the inertization process include an insufficient stabilisation of incorporated HEs, as indicated by the high hazard quotients (beyond the permissible limits established for inert materials) obtained in some cases for Mo, As, Cr, Pb, and Cu elements. Such behaviour is related to oxy-anionic complexes (Mo, As, Cr) that can form their own phases or are not linked to the tetrahedral framework of aluminosilicate glass. Pb and Cu elements are preferentially partitioned to glass with a low coordination

number, while As and especially Mo are not stabilised in silicate ceramics. These drawbacks necessitate conducting additional studies to develop appropriate inertisation strategies for these elements.

Graphical abstract
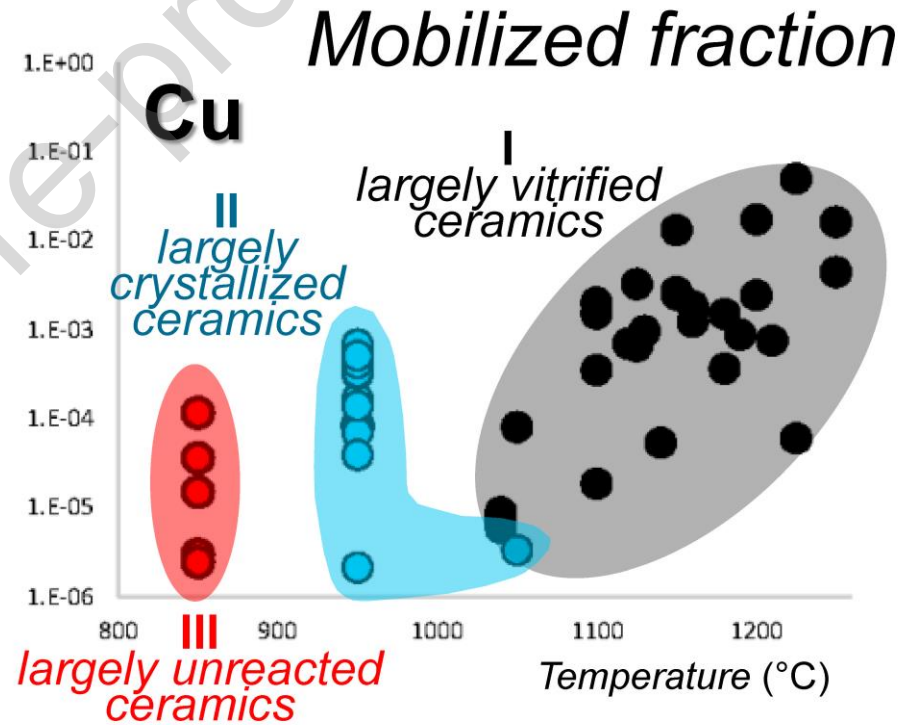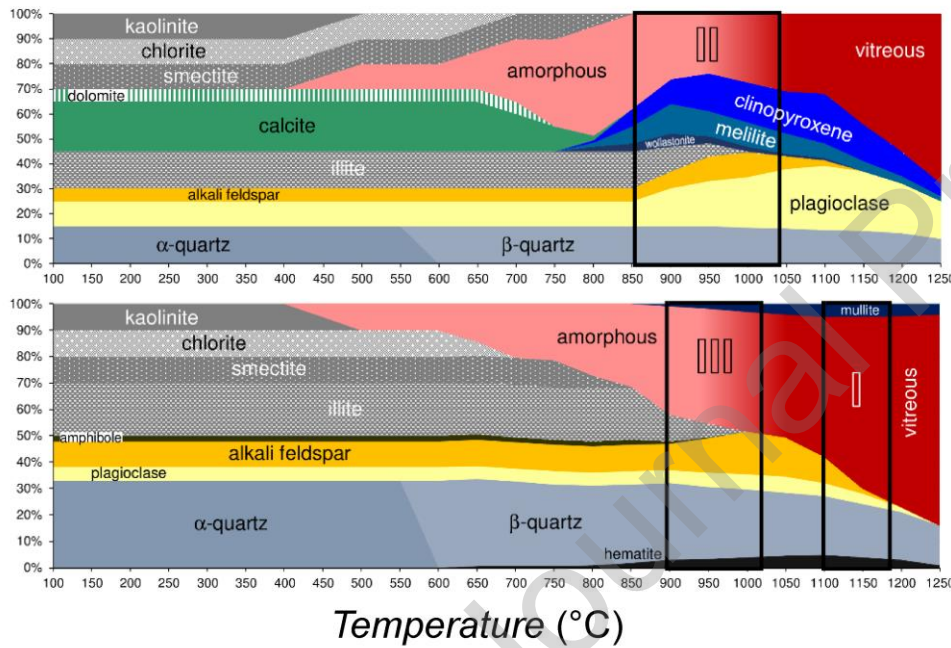
Keywords: immobilisation efficiency; element mobility; firing behaviour; inert materials

1. Introduction

Waste recycling can potentially become a common practice for improving the environmental sustainability of the manufacturing process. This approach is feasible only in the case of high-throughput production, such as the fabrication of bricks and roof tiles, wall and floor tiles, lightweight aggregates, whiteware, and materials that can endure the undesired effects induced by waste addition. The growing interest of both industrial and academic researchers working on waste valorisation is supported by the hundreds of technological studies conducted in this field (Dondi et al., 1997; Coronado et al., 2015; Andreola et al., 2016; Dondi et al., 2016; Al-Fakih et al., 2019). Although numerous tests have been performed in the ceramic industry, their results mostly remain unpublished. This tendency is expected to strengthen once the transition towards a circular economy is fully implemented (Kalmykova et al., 2018; Andreola et al., 2020).

In any case, it is necessary to introduce an increasing amount of waste materials into ceramic batches (such as pre-consumer and post-consumer residues) to overcome the currently used cannibalistic loops which re-use scraps within the same manufacturing process. This option would significantly broaden the compositional spectrum of natural raw materials, including hazardous ones (Coronado et al., 2015; Dondi et al., 2016; González-Corrochano et al., 2018; Andreola et al., 2019; Al-Fakih et al., 2019).

The incorporation of waste into a ceramic body is an effective way to stabilise hazardous materials, as demonstrated in recent reviews (Karayannis et al., 2017; Kinnunen et al., 2018; Hossain and Roy, 2020; Zhang et al., 2021; Zhao et al., 2021) and several research studies (Bernardo et al., 2006; Raimondo et al., 2007; Alonso-Santurde et al., 2011; Haiying et al., 2007, 2011; Quijorna et al., 2011; Tan et al., 2012; Martinez et al., 2012; Pérez-Villarejo et al., 2015; Tang et al., 2019). However, a quantitative estimation of the degree of immobilisation of dangerous elements during the manufacturing of silicate ceramics has been rarely conducted in the past, while the majority of published papers mainly focus on technological issues. In some cases, the mobility of hazardous components was investigated as part of ceramic processing (Coronado et al., 2015; González-Corrochano et al., 2018; Zanelli et al., 2021). This situation reflects the lack of regulations regarding the release of hazardous elements (HEs) from finished

3

ceramic products apart from the currently existing standards regulating the release of Pb and Cd elements from ceramic items intended to be in contact with food. This is due the fact that silicate ceramics are fabricated from natural raw materials which contain only trace amounts of HEs.

Overall, the published literature works describe the immobilisation of dangerous elements in specific cases that are difficult to generalise due to the different processing conditions and material compositions. A systematic evaluation of the degree of HE immobilisation in silicate ceramics has not been performed yet because it requires a better understanding of the mechanism of the immobilisation process. Although this question is of paramount importance for developing novel waste recycling strategies, it has been rarely addressed in the literature (Dondi et al., 2002; Magalhães et al., 2004; García-Valles et al., 2007; Karnis and Gautron, 2009; Tang et al., 2019; Coronado et al., 2015; González-Corrochano et al., 2018; Mao et al., 2018). A necessary step includes a quantitative assessment of the ceramisation efficiency of HEs incorporated into silicate ceramics, here attempted for the first time as a critical assessment of the literature. The subsequent studies would require a proper background on the composition and processing conditions of ceramic products to outline how the phase transformations occurring during ceramic manufacturing can affect the inertisation efficiency, which is the novelty of our approach. The potential impact of this work includes a paradigm shift from the empirical approach commonly used in waste recycling to a novel strategy of batch design, which is based on the observed HE behaviour in various silicate ceramics.

The objective of the present work is to quantitatively determine if the benefits of incorporating HEs into silicate ceramics outweigh the pitfalls, especially those affecting the efficiency of the ceramisation process. The utilised analysis procedure involves the following four steps:

a) Identification of HEs that can potentially be immobilised by silicate ceramics with a special attention to toxic components;

b) Parameterisation of the immobilisation degree of HEs after their incorporation into a ceramic matrix;

c) Description of different ways for immobilising a particular element in a ceramic matrix, which considers the reactions that occur during firing;

d) Evaluation of the literature case studies devoted to waste recycling in silicate ceramics to identify the benefits and pitfalls.

2. Methodology

This section describes the methodological approach utilised to select suitable HEs for silicate ceramics and proposed parameters for evaluating their degree of immobilisation in ceramic matrices. In addition, various criteria for selecting case studies on the mobilisation of dangerous elements after waste recycling are discussed, including those used to classify different types of silicate ceramics.

2.1. HEs in silicate ceramics

No regulations regarding the use of HEs in silicate ceramics and limits of their potential release have been established. There is a single exception of Pb and Cd elements in ceramic items that are intended to be in direct contact with food. Various standards related to determination methods and limits of acceptance for the release of Pb and Cd elements have been developed in many countries, such as the international standards for ceramic tiles (ISO 10545-15, 1995) and tableware (ISO 6486-1, 2019). The permissible limits used in the European Union are 4 mg·L^{-1} (Pb) and 0.3 mg·L^{-1} (Cd), although these values may be lowered in the future.

Other local regulations exist as well, such as *California's Safe Drinking Water and Toxic Enforcement Act* of 1986 (Proposition 65) which requires to declare if any HEs are contained in a given product. In addition to Cd and Pb elements, this proposition includes Ni and some forms of Co and V elements.

In such a situation, a reasonable approach would be based on the existing legal framework, which is more comprehensive and better structured than other standards used for ceramic products, such as the waste classification for landfilling. It is noteworthy that this approach was adopted in several studies (Quijorna et al., 2011; Schabbach et al., 2012; Liu et al., 2019) by considering the limits established for inert materials. These limits vary significantly from country to country (see Table 1) and, consequently, affect the definition of inert materials.

Table 1.

The HEs listed in Table 1 are not the only components of concern, as other elements are also considered toxic by national laws, including Co, V, Sn, and radioactive elements. Hence, this list of HEs can be considerably extended to include the following common ingredients of ceramic glazes and pigments: Co, Ni, Ba, Cr, Sb, and Zn. In addition, it contains components of colourants and additives that have a limited use in silicate ceramics, such as Cd, Sn, V, Ag, Cu, Mo, and Se. In principle, Pb, As, and Hg are banned by the ceramic industry and should not be present in significant amounts in industrial minerals; however, they may be found in secondary raw materials and by-products. The limits listed in Table 1 decrease in the following order: Ba, Zn, Cu, Cr, Mo, As, Pb, Ni, Se, Sb, Cd, and Hg. This trend implies an order of increasing danger from Ba to Hg, which is taken into account by the rules and regulations adopted in all countries.

In addition to the aforementioned HEs, the volatile compounds that can be released in the form of flue gases during the firing of silicate ceramics represent a significant environmental problem. These components include fluorine compounds (mostly HF), chlorine compounds (HCl, Cl_2), sulphur oxides (SO_2, SO_3), nitrogen oxides (NO, NO_2), volatile organic compounds, and particulate matter (Palmonari and Timellini, 1982; Minguillón et al., 2009; Monfort et al., 2011; Rajarathnam et al., 2014; Ferrari and Zannini, 2017; Akinshipe and Kornelius, 2017). Such emissions monitored by industrial furnace chimneys must comply with the limits legally adopted in various countries. However, the discussion of gaseous emissions is beyond the scope of the present study and will not be considered here. Therefore, only the HEs for which sufficient data are available from the literature studies on silicate ceramics (phosphate or oxide ceramics are not considered), are discussed in this work. These elements include As, Ba, Cd, Cr, Cu, Mo, Ni, Pb, Se, Sb, and Zn. Published data on Hg (Haiying et al., 2011; Pan et al., 2015; Vieira et al., 2016) do not provide all the necessary information, and, to the best of our knowledge, there are no accessible data regarding the mobilisation of Be, Ag and radioactive elements in silicate ceramics. On the other hand, there is a wide literature on the stabilisation of radioactive residues, which also includes glassy and glass-ceramic

systems with some analogy to silicate ceramics. For this issue, the reader is addressed to the specific literature (Ewing and Lutze, 1991; Lee et al., 2006; Donald, 2010; McCloy and Goel, 2017).

2.2. Parameterisation of inertisation efficiency

The assessment of inertisation efficiency involves the determination of an extent to which a given HE is mobilised during storage or operational conditions for silicate ceramics. According to the literature, the results of leaching tests can be used to measure the degree of HE mobilisation (Loncnar et al., 2016; Donatello et al., 2010; Galvín et al., 2012).

Many different methodologies and standards have been developed for leaching tests (such as the regulatory, standard, and research leaching methods). Regardless of the testing procedure, leaching can be performed by a static extraction or *batch tests*, in which the leaching fluid is added once, or by dynamic extraction or *column tests*, in which the extraction fluid is renewed during the process (Tiwari et al., 2015; Krüger et al., 2012). During a batch test, a sample is placed into a fixed volume of leaching solution. The contact between the particle surfaces and the fluid is achieved by continuous mixing. After a certain time, the leachate concentrations reach those obtained at the equilibrium conditions (Tiwari et al., 2015; Galvín et al., 2012). The column tests conducted for continuous leaching are expected to be more accurate during the simulation of the real environmental conditions, better reflecting the properties of the fluid involved in HE transport. However, these tests are not considered here because they are too sensitive to experimental conditions (Tiwari et al., 2015). In general, suitable research methods should be able to reproduce the waste leaching potential in a specific application (Yin et al., 2018), and it is difficult to compare the leaching data obtained by different procedures to quantify the hazards associated with a particular waste product. It is well known that changes in experimental parameters (such as solution pH, liquid/solid ratio, leaching reagents, redox and microbial activities, reaction time, and temperature) can strongly affect the leaching test results (Al-Abed et al., 2008; Yin et al., 2018). However, metal leaching parameters can strongly depend (even for a single analytical procedure) on the waste matrix properties,

which may in turn influence the interaction of leaching components with dissolved minerals to induce sorption, secondary reactions, and re-precipitation (Tiwari et al., 2015). Despite these limitations, a comparison of HE mobilities obtained from the leaching data for fired products, is considered the best way of achieving a better understanding of the effect of ceramisation on HE inertisation and predicting a potential hazard. However, any discussion of the significance and reliability of leaching tests is beyond the scope of the present study. Thus, the data reported for silicate ceramics have been taken into account.

Based on the obtained leaching test results, the following three parameters are proposed for HE characterisation:

i) the efficiency of HE immobilisation,

ii) the mobilized HE fraction, and

iii) the hazard quotient.

These parameters allow contrasting leaching data (which are usually compared with permissible limits of release) with the total amount of every HE present in the ceramic body. The *efficiency of immobilisation* (ε_{HE}) expresses the percentage of a given HE that is not mobilised during the leaching test of the waste-bearing ceramic bulk:

$$\varepsilon_{HE} = \frac{(\xi_{total} - \xi_{leached})}{\xi_{total}} \cdot 100 \qquad (1)$$

where ξ_{total} and $\xi_{leached}$ are the HE weight contents in the bulk and leachate, respectively. The $\xi_{leached}$ values are calculated from the measured HE concentrations in the leachate solution and then normalised with respect to the extraction volume determined by a specific procedure. By utilising this approach, it is possible to calculate the required efficiency of immobilisation as a function of the HE concentration in the ceramic batch from the maximum leachate concentration specified by regulations (Fig. 1). Notably, the calculated required efficiency increases exponentially with ξ_{total}; for

8

instance, in the case of a 0.1% concentration in the batch (HE oxide), it spans from $\varepsilon_{Ba} = 97.8\%$ to $\varepsilon_{Cd} = 99.996\%$. If the amount of HE in the bulk is as

high as 1 wt.%, the required efficiency must vary from $\varepsilon_{Ba} = 99.78\%$ to $\varepsilon_{Cd} = 99.9995\%$.
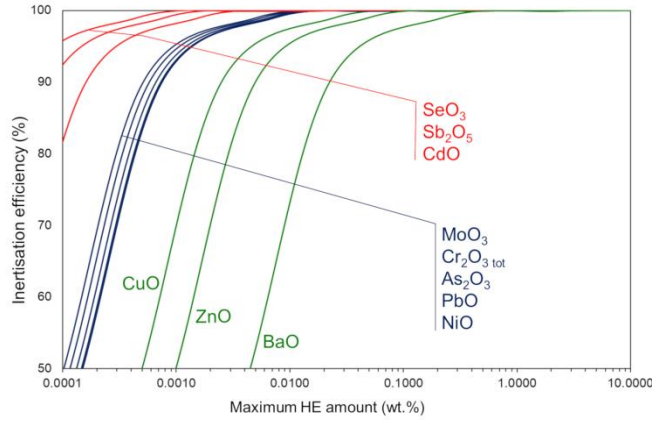

Figure 1.
Another parameter used to quantify the degree of retention of toxic elements in silicate ceramics by conducting leaching tests is the *mobilised fraction*

(f_{HE}), which represents the fraction of HEs that can be released to the total HE amount:

$$f_{HE} = \frac{\xi_{leached}}{\xi_{total}}$$ (2)

where $\xi_{leached}$ and ξ_{total} are the relative HE weight fractions in the leachate and ceramic bulk, respectively. Using this formula, it is possible to determine

the relationship between the maximum f_{HE} allowed by EU regulations as a function of the HE concentration in the ceramic matrix (Fig. 2). For

instance, at a high HE oxide content of 1 wt.%, the maximum HE fraction that may be released into the leachate varies from $f_{Ba} = 0.002$ to $f_{Cd} <$

0.00001.

9

Both the ε_{HE} and f_{HE} values suggest that the current waste recycling regulations are very tight, as HEs must be retained with extremely high efficiency. In the case of relatively large amounts of HEs in a ceramic batch (>1 wt.% for HE oxides), the efficiency of immobilisation often exceeds 99.9%.
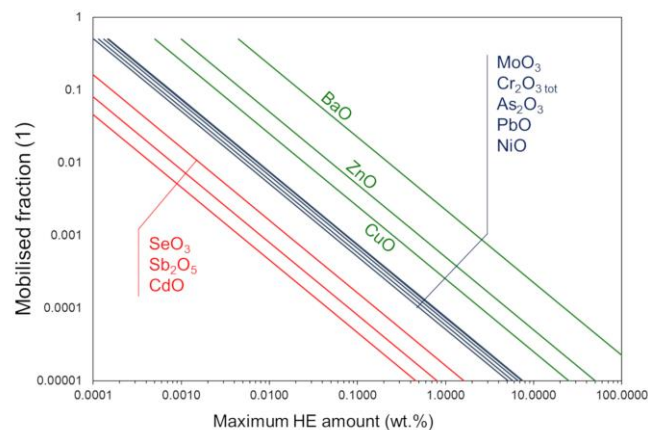

Figure 2.

The *hazard quotient* (HQ_{HE}) is expressed by the following ratio:

$$HQ_{HE} = \frac{\xi_{leached}}{\xi_{limit}} \tag{3}$$

This metric shows how close is the released HE amount ($\xi_{leached}$) to the regulatory limit established for inert materials (ξ_{limit}). Similar to $\xi_{leachate}$ values, ξ_{limit} takes into account the solvent volume, allowing a comparison of results obtained by different methods. The HQ_{HE} values above unity indicate that the permissible limit is exceeded. It is useful for calculating differences with respect to leaching thresholds. This parameter was primarily defined by the US Environmental Protection Agency (US EPA, 1989) to assess the health risks of air toxic compounds as the ratio between the exposure concentration for a given compound and a reference concentration without a significant risk of harmful effects. The HQ values greater than one do not represent a statistical probability of the occurrence of a harmful event; they simply indicate that the exposure concentration exceeds the reference

10

concentration. Subsequently, the hazard quotient has been used in many studies on the presence and release of HEs from different materials (Yousaf et al., 2017; Golge et al., 2018; Saba et al., 2019; Yang et al., 2021).

2.3.   Selection of literature case studies

Literature studies on waste recycling in silicate ceramics have been reviewed to determine how the batch composition and firing conditions can affect the inertisation of HEs. A selected paper has to include relevant data (leaching results, waste and body compositions, firing schedules) in order to calculate the inertisation efficiency according to the procedure outlined in section 2.2, and classify silicate ceramics as described in section 3.2. Specifically, silicate ceramics constitute different cases according to the phase transformations occurring during heat treatment (more details are provided in section 3.2). In this work, we considered the following three cases:

I) *Largely vitrified products*, which are mainly represented by porcelain stoneware and stoneware tiles, sanitary ware and other porcelain types, and lightweight aggregates.

II) *Largely recrystallised products*: pottery, bricks, and tiles containing high-CaO and/or high-MgO bodies (such as earthenware, majolica, and monoporosa); and

III) *Largely unreacted products* mainly consisting of residual and amorphous phases, such as pottery, pipes, bricks, and tiles with low-CaO and/or low-MgO bodies.

As a result, twenty-five papers have been selected, and the main parameters of these case studies are summarised in Table 2. Overall, the listed samples constitute a relatively large data set, although the obtained matrix is not fully representative of all ceramic products, types of batches, and firing temperatures.

Table 2.

3. Results

This section describes the meta-analysis data obtained for two bodies of literature including 1) case studies on the inertisation of HEs for waste recycling in silicate ceramics and 2) factors affecting the behaviour of ceramics as HE acceptors.

3.1. Case studies

The selected literature provides a data population that varies with HE, although in most cases, information is available for all types of silicate ceramics and a relatively wide range of firing temperatures. This is true for Zn, Cr, Ba, Cu, Pb, and As elements (over 50 data points each) and, to a lesser extent, for Ni and Mo (35 data points each). In contrast, only small numbers of data points are available for Cd (17) and especially for Se and Sb (6 and 4 samples, respectively). The ranges of concentrations for HEs considered in this study are provided in Fig. S1 (Supplementary Materials).

These literature data do not cover various industrial products and types of silicate ceramics with the same frequency. In fact, the selected case studies include mainly wall and floor tiles (8), clay bricks (7), and glass ceramics (3) among different ceramic products. Regarding the type of ceramics, data are reported for largely vitrified bodies (class I, 22 samples), largely recrystallised bodies (class II, 22 samples), and, to a lesser extent, for largely unreacted bodies (class III, 7 samples).

The analysed waste sources are obtained from six sectors: metallurgical (Waelz slag, electric arc furnace slag, foundry sand, and stainless steel dust; 15 samples); biomass and solid waste incineration (bottom and fly ashes; 14 samples); wastewater treatment (including sewage and galvanic sludge; 13 samples); waste glass recovery (panel and soda-lime glasses including mixed ceramic and glass residues; 5 samples); mining and mineral

transformation (solid petroleum waste and sludge from alumina, titania, and chromite production; 4 samples), and dredging (harbour sediment, 4 samples).

The firing temperatures vary over a wide range from 850 to 1250 °C. An anticipated correlation between the maximum temperature and the silicate ceramic type has been confirmed: largely unreacted bodies (class III) were fired at 850 °C with a single case fired at 1020 °C. Largely recrystallised bodies (class II) usually required maximum firing temperatures in the range of 930–1025 °C with four cases spanning from 1050 to 1100 °C (mostly glass ceramics). Largely vitrified bodies (class I) were sintered between 1120 and 1240 °C.

3.1.1. Mobilised HE fraction

The mobilised HE fraction is plotted as a function of the firing temperature for largely unreacted, largely recrystallised, and largely vitrified silicate ceramics in Fig. 3. The degree of retention of toxic elements inside the ceramic matrix and its dependence on temperature/type of product differ for various HEs. These plots show the existence of a different behaviour for specific HEs.

i) HEs with low mobilised fractions (Ba, Pb, Ni, and Zn with average $f_{HE} \leq 0.002$), which demonstrate no apparent correlation between f_{HE} and the firing temperature/product type.

ii) HEs characterised by a medium-high degree of mobilisation on average: the highest value is obtained for Mo ($f_{Mo} = 0.43$) and the lowest ones for Cd ($f_{Cd} = 0.01$) and Cr ($f_{Cr} = 0.003$). Also in this case, it was not possible to observe any correlation between the mobilised HE fraction and the firing temperature.

iii) HEs with degrees of mobilisation varying from low to high values. For this group, the mobilised HE fraction is strongly correlated with the firing temperature. For example, for As and Cu elements (with maximum $f_{As} = 0.23$), the increase in the firing temperature increases their mobilised fractions. As a result, As and especially Cu are more mobilised in largely vitrified ceramics.
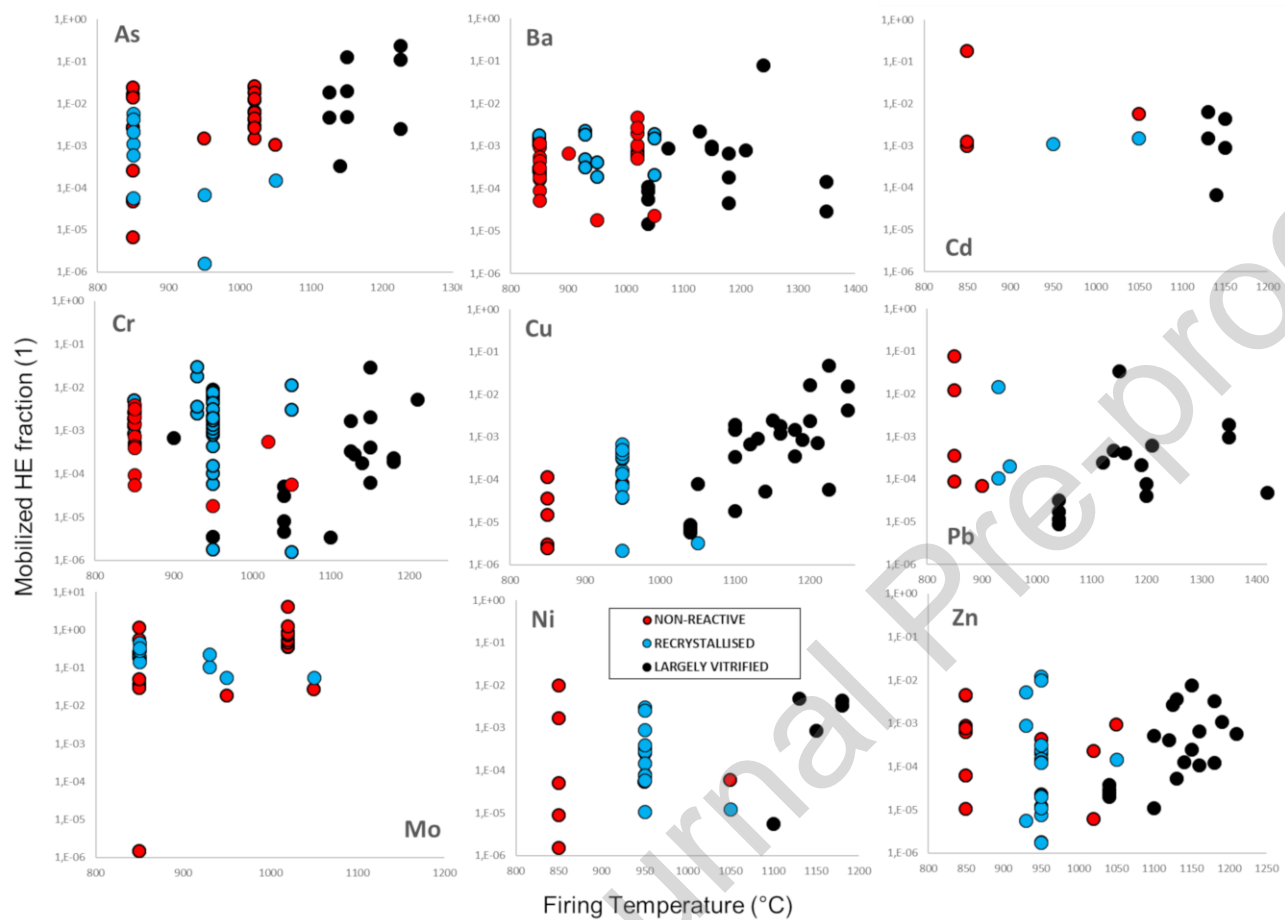
13

Figure 3.

3.1.2. Hazard quotient

The hazard quotient (HQ_{HE}) is plotted as a function of the firing temperature for different types of silicate ceramics in Fig. 4. For the majority of the

analysed cases, its computed values are relatively low, indicating that the studied HE concentrations are within the permissible limits established for

inert materials by regulatory agencies. This is particularly true for Ba, Cd, and Se whose HQ_{HE} values range, on average, from 0.01 to 0.08. Other HEs, such as Cu, Ni, and Zn, possess higher hazard quotients (0.14 < HQ_{HE} < 0.33 on average), although their $\xi_{\text{leached}}/\xi_{\text{limit}}$ ratios rarely exceed unity. A different situation is observed for As, Sb, Pb, Cr, and Mo elements, which exhibit the highest values of this index. In particular, the average HQ_{Pb}, HQ_{Cr}, and HQ_{Mo} magnitudes are in the 1.1–5.9 range, suggesting particular caution when recycling these HEs as their significant amounts can be released from unreacted and recrystallised silicate bodies.
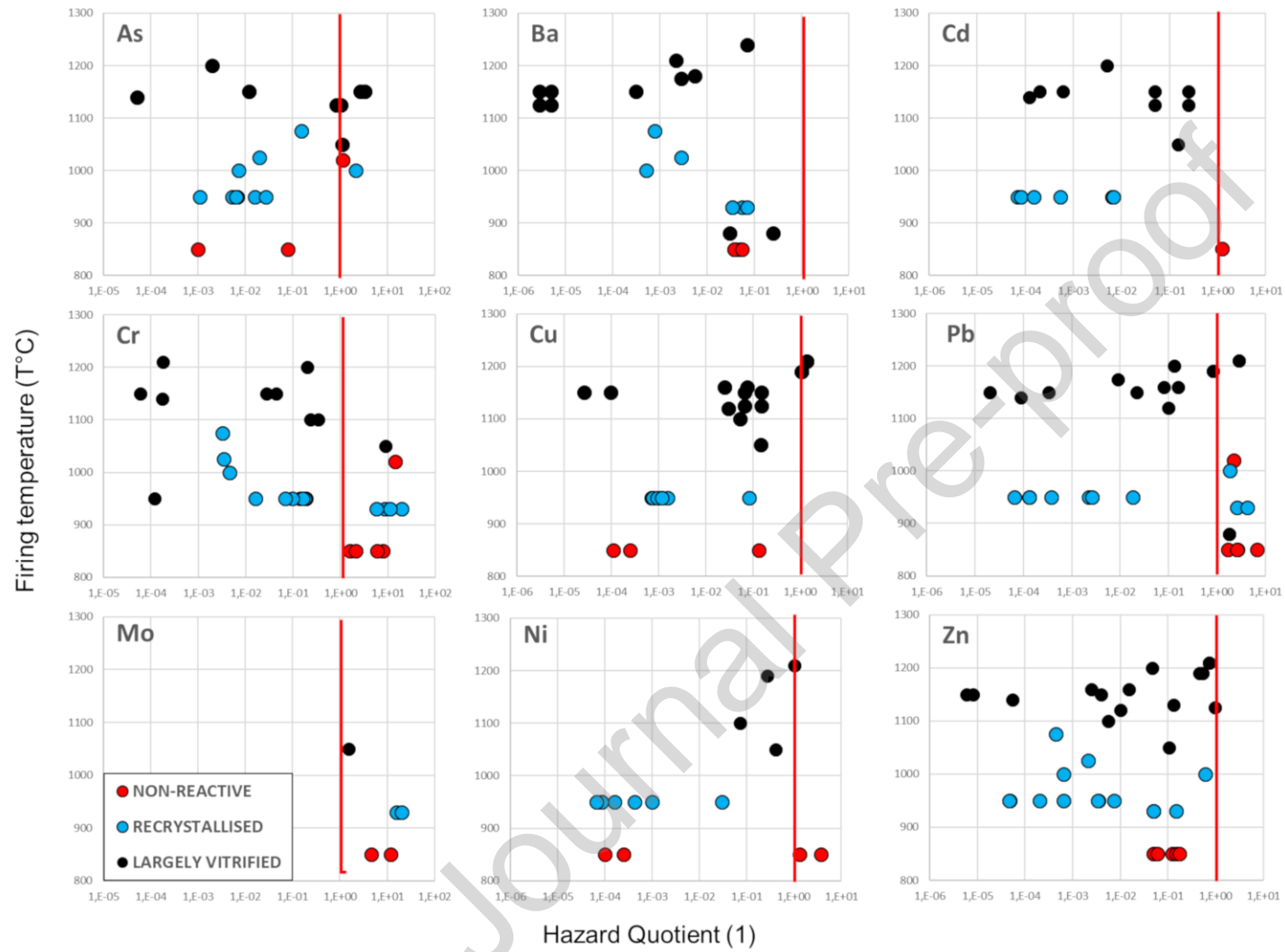
Figure 4.

3.1.3. Immobilisation efficiency

The efficiency of immobilisation is plotted as a function of the HE concentration in ceramic batches in Fig. 5. Overall, silicate ceramics exhibit high HE immobilisation efficiencies. This is particularly true for Ba, Cd, Ni, and Zn elements, which have only three cases with ε_{HE} < 99%. However, the lowest efficiencies of immobilisation are observed at the following HE oxides concentrations in the batch: from ~0.0001% CdO to ~0.01% NiO and to ~0.1% BaO up to ~1–4% ZnO. Meanwhile, Cr, Cu, and Pb elements have few samples within 90% < ε_{HE} < 99%. Such cases of relatively low immobilisation efficiencies are observed for the batches with Cr_2O_3 and PbO concentrations of approximately 0.01%, while in the case of Cu, small immobilisation efficiencies are obtained at both very low (~0.001%) and extremely high (~25%) CuO contents. As and especially Mo elements display some values with ε_{HE} < 90%. In these cases, the As_2O_3 and MoO_3 concentrations in the batch varied between 0.001% and 0.01%.
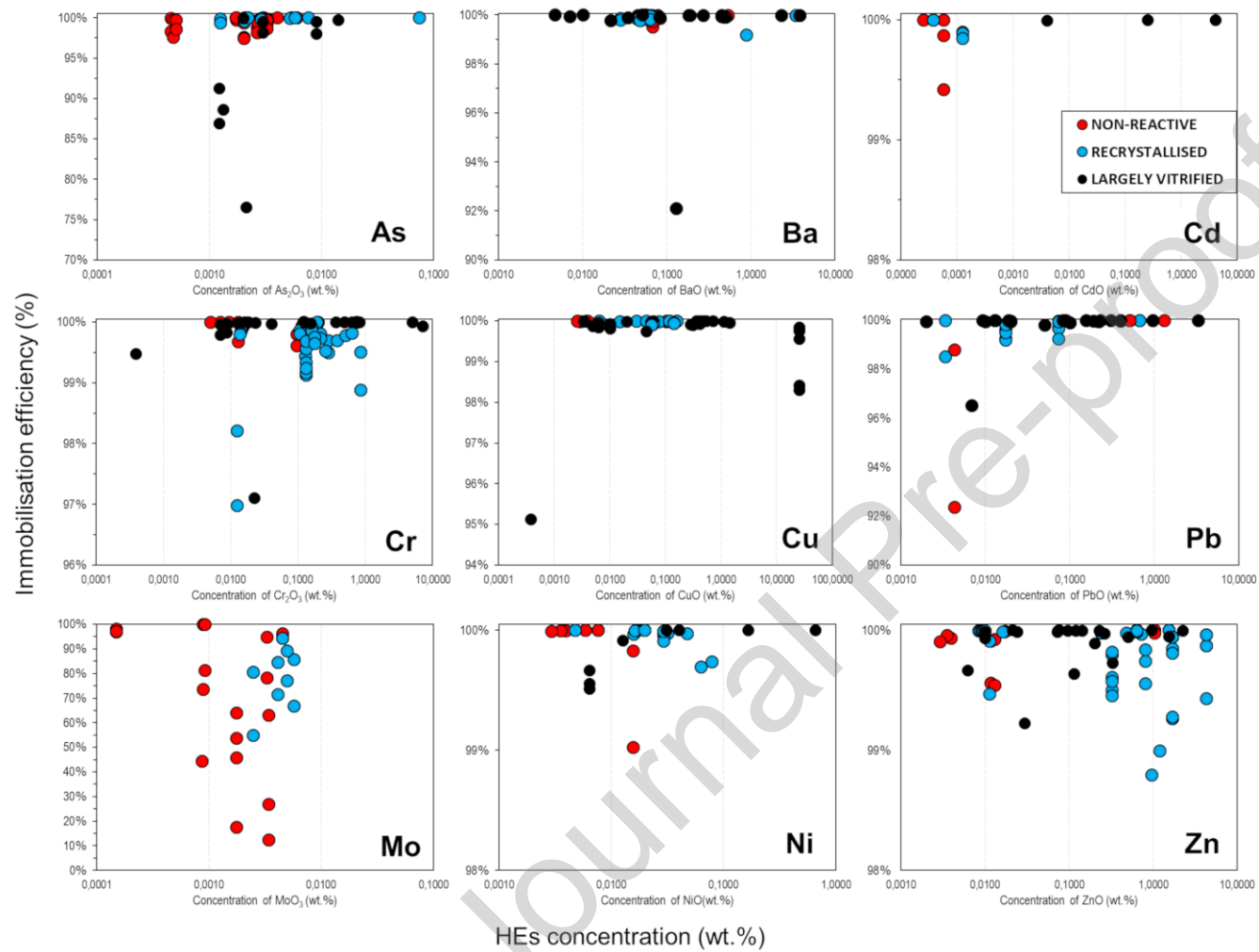
17

Figure 5.

3.2. Silicate ceramics as waste acceptors

Silicate ceramics are composed of heterogeneous bodies: a mixture of various minerals that undergo phase transformations during processing, especially at the firing stage. This is favourable for the waste incorporation because a highly heterogeneous mix is intrinsically prone to accommodating extraneous components. At any rate, waste is increasingly tolerated as far as its technological behaviour resemble those of conventional raw materials (Coronado et al., 2015; Cifrian et al., 2019; Zanelli et al., 2021). This practice, which is substantially based on technological issues, does not ensure that HEs are immobilised as efficiently as residues are incorporated into silicate ceramics.

To achieve a satisfactory degree of immobilisation, it is necessary to accommodate HEs inside crystalline or amorphous ceramic components. Hence, the stabilisation process involves the incorporation into phases that must be able to endure hydrolysis or chemical attack during utilisation of silicate ceramics. Such an incorporation occurs in the firing process, when new compounds are formed and HEs can be allocated to either a crystalline lattice or glassy networks of vitreous phases. However, if this process is not complete, HEs may remain in their original form in the waste or weakly retained in the amorphous or low structural order phases. In this context, waste stabilisation treatments can play an important role, especially at high HE concentrations (Schabbach et al., 2012; Andreola et al., 2019; Andreola et al., 2020). This picture implies different chemical and physical stabilisation conditions that reflect in the degree of HEs mobilization. Note that some HEs maintain their original valence states and structural allocations (e.g. Ba^{2+}, Zn^{2+}, Cd^{2+}), while other HEs can assume multiple valences and participate in redox reactions (such as $Cr^{3+} \leftrightarrow Cr^{6+}$, $Mo^{3+} \leftrightarrow Mo^{6+}$, $V^{3+} \leftrightarrow V^{5+}$, and intermediate valence states).

Thus, the goal of increasing the inertisation efficiency is to maximise the incorporation of HEs into the phases formed during the firing process, which ensures their high chemical stability in water. This behaviour is expected for crystalline silicates and aluminosilicate glasses present in ceramics.

The principal phase transformations of three silicate ceramics occurring during heat treatment are described in Figure 6.
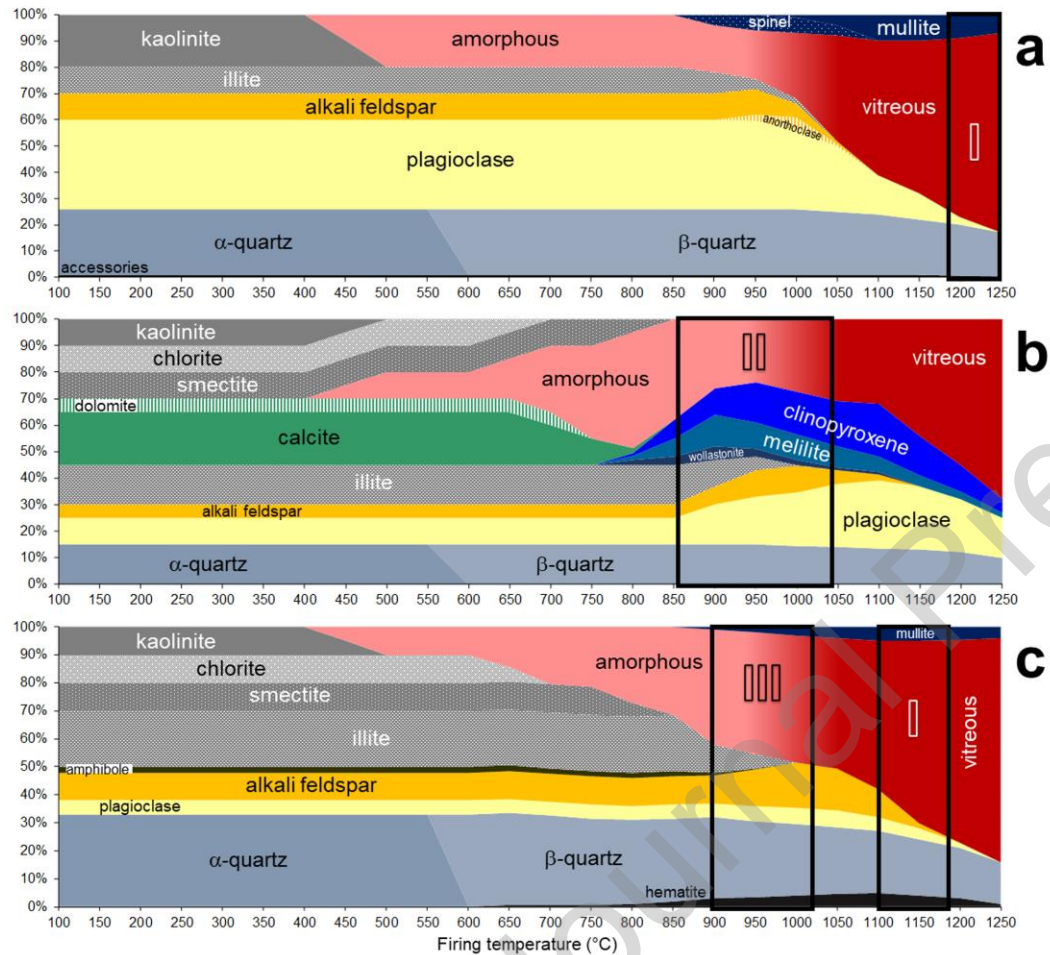
Figure 6.

I) *Largely vitrified products* whose main high-temperature reactions include melting feldspars and illite-mica with a partial involvement of quartz (Gualtieri, 2007; Bernasconi et al., 2014; Conte et al., 2020) and the incorporation of amorphous by-products derived from the breakdown of clay minerals (Figs. 6a and c). This melt generates an abundant vitreous phase in the finished products (Zanelli et al., 2011; Bernasconi et al., 2016).

20

Kaolinite first transforms into an amorphous phase and then (at approximately 1000 °C) into mullite with possible intermediate compounds, such as γ-Al_2O_3 or a (Si,Al) spinel-like phase (Bellotto et al., 1995; Gualtieri and Bellotto, 1998). The main challenge here is the impossibility of directly controlling firing reactions, and only their side effects can be monitored by manufacturers (for instance, variations in the product size or porosity).

II) *Largely recrystallised products*, which undergo a complex set of transformations with increasing temperature, promoting the clay minerals breakdown into disordered phases and carbonate decomposition into calcium and magnesium oxides (Fig. 6b). The resulting by-products react with each other at temperatures above 800 °C to generate various calcium and magnesium silicates and aluminosilicates according to kinetic constraints (Cultrone et al., 2001; Heimann and Maggetti, 2019). The crystalline phases formed during firing commonly include anorthite-rich plagioclase (Ballato et al., 2005; Ouahabi et al., 2015); fassaitic clinopyroxene, a diopside rich in Al and Fe (Dondi et al., 1998; Cultrone et al., 2001); and complex melilites consisting of gehlenite–åkermanite–ferrigehlenite solid solutions (Dondi et al., 1999a). Other newly formed phases such as wollastonite, periclase, spinel, larnite, and rankinite may be also present in small amounts. In the usual firing range, quartz and feldspars are relatively stable, while illite-mica is stable at temperatures up to approximately 1000 °C. A minor amount of the amorphous phase can be also present in the finished products (Dondi et al., 1999b).

III) *Largely unreacted products* that are fired at relatively low temperatures. At these firing conditions, quartz, feldspars and micas are stable, and only limited transformations may occur (Dondi et al., 1999b; Heimann and Maggetti, 2019), leading to the formation of amorphous or disordered phases from clay minerals transformation (Fig. 6c). The newly formed crystalline phases typically include hematite and some mullite or spinel species (Cultrone et al., 2005).

A representative diagram of the phase composition of silicate ceramics is shown in Figure 7.
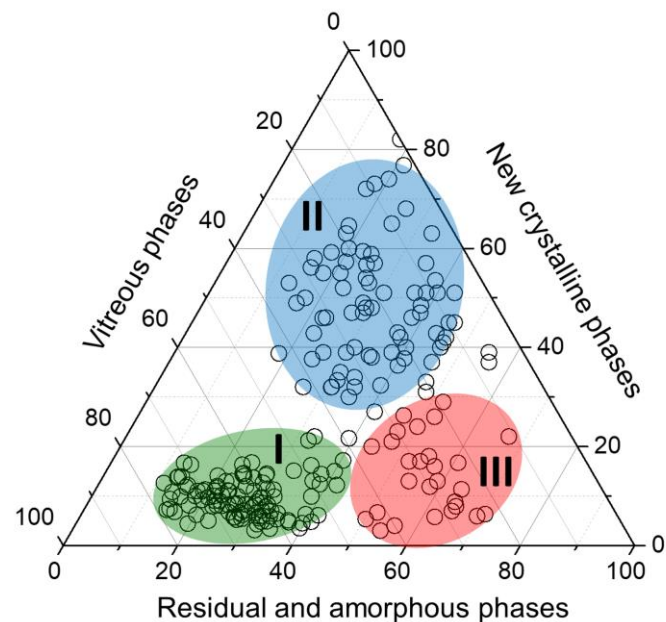
Figure 7.

During the firing process, HEs can be either incorporated into the newly formed phases or retained in the original compound of the waste material if they are thermally stable. Although kiln burners are usually fed with an almost stoichiometric methane–air mixture, ceramic furnaces always have an auxiliary air supply which ensures that the oxygen fugacity is sufficiently high. Therefore, the kiln atmosphere may favour the formation of higher valence states for some HEs. This can occur in the case of Cr^{6+} (Abreu and Toffoli, 2009), which implies a higher risk of generating toxic by-products. In the former case, HEs may be hosted either in crystalline compounds lattice or into the vitreous phase (or both). In this process, they compete with other major and minor elements of ceramic bodies. The preference of each HE for a given crystalline or amorphous phase essentially depends on the crystal chemistry or glass chemistry factors derived from different structural environments where a certain ion can be allocated (Lu et al., 2017, 2019).

These factors also affect the competition between various HEs present in the same waste. However, the presented data consider each HE individually, because no information is available on the mutual effects attributable to two or more heavy metal ions.

The newly formed crystalline phases contain a variety of structural sites that can host HEs. These structural sites are characterized by different metal–oxygen mean bond distances, polyhedral volumes, polyhedral distortion indexes (including quadratic elongations and angle variance), and effective coordination numbers, as shown in Fig. 8 for plagioclase-celsian, orthoclase, clinopyroxene, melilite, mullite, and spinel. These sites can form large polyhedra with the central ion usually coordinated by 8–12 surrounding oxygen ions, where divalent alkali earth metals and ions of other HEs with large ionic radii can be accommodated. This is observed for melilite (both tetragonal and monoclinic polymorphs), celsian, and orthoclase crystal structures, in which Ba^{2+} ions can be easily hosted at the cubic sites (Shimizu et al., 1995; Ardit et al., 2012a; Rocquefelte et al., 2007; Viswanathan and Brandt, 1980) or feldspars, where Pb^{2+} is hosted at the cubic site of the orthoclase lattice. However, in the latter case, the coordination number is reduced from seven (that of strontium feldspar cubic site) to six (Benna et al., 1996). Other crystal structures, such as clinopyroxene, spinel, and mullite, can host several HE ions (most of them are divalent and trivalent transition metal ions) at octahedral sites. For instance, Cr^{3+} may be hosted in all the aforementioned structures (Clark et al., 1969; Lenaz et al., 2004; Fischer and Schneider, 2000), and Ni^{2+}, Cu^{2+}, Zn^{2+}, and V^{3+} ions can be accommodated at the clinopyroxene (Raudsepp et al. 1990; Redhammer et al., 2005; Redhammer and Roth, 2005; Ohashi et al., 1994) and spinel (Yamanaka, 1986; Jarrige and Mexmain, 1990; O'Neill and Dollase, 1994; Bosi et al, 2016) octahedral sites. In some cases, spinels with certain chemical compositions can host octahedrally coordinated Cd^{2+} (Allali et al., 2014) and Ni^{3+} (Shafer, 1962) ions. The small tetrahedral sites of feldspar, clinopyroxene, and mullite crystal structures, preferentially occupied by Si^{4+} or Al^{3+} ions, preclude the incorporation of HEs. Meanwhile, HEs such as Cu^{2+} and Zn^{2+} can be hosted at the relatively large tetrahedral sites of the melilite (Du et al., 2003; Ardit et al., 2012b; Malinovskii, 1984; Kaiser and Jeitschko, 2002) and spinel (Sinha et al., 1957; O'Neill and Dollase, 1994) lattices. The extreme versatility of the spinel

23

structure also allows the incorporation of Cu^+ (Jarrige and Mexmain, 1990), Ni^{2+} (Kiselev et al., 2007), V^{4+} (Rüdorff and Reuter, 1947), and Mo^{6+} (Fortes, 2015) ions at its tetrahedral sites.
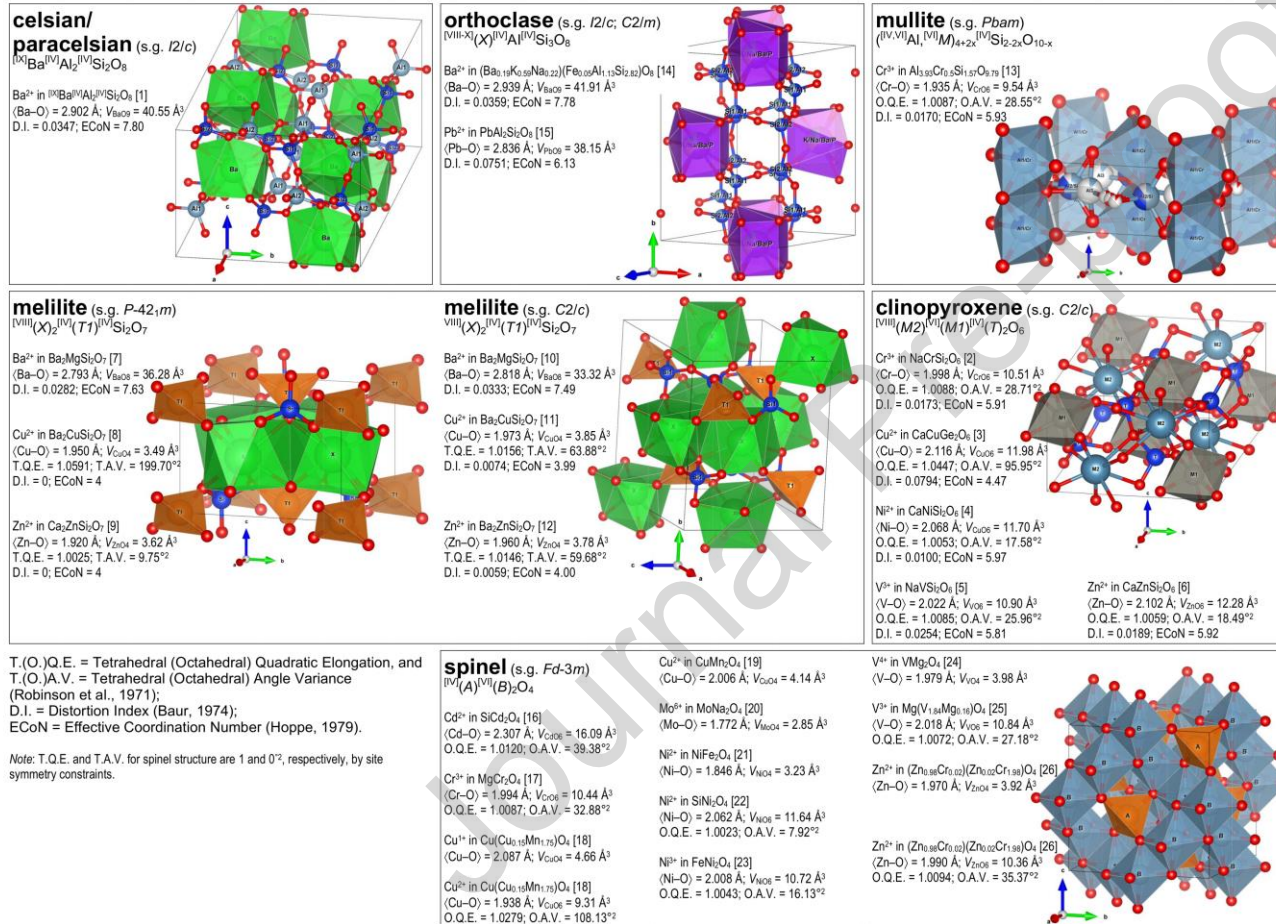

Figure 8.

The vitreous phases formed in silicate ceramics are aluminosilicate glasses (melts at high temperature), whose composition depends on the ceramic body and firing conditions (Conte et al., 2020). However, the glass composition is currently determined only for porcelain stoneware and porcelain (Carty and Senapati, 1998; Zanelli et al., 2011) and resembles that of peraluminous granitic melts. In stoneware bodies, the melt is richer in Fe and alkali-earth elements as compared with whitewares, and its composition is close to those of dacitic–andesitic melts. Overall, the vitreous phases present in silicate ceramics can accommodate HEs under certain conditions, including the valence state, oxygen coordination, metal–oxygen distance, and possible formation of complexes (Mysen and Richet, 2018). These structural characteristics imply a different degree of HEs incorporation into the glass network, with implications on ease of removal by acid attack and consequently the leaching behaviour (Kim et al., 2020). Such conditions may be obtained from the published literature studies on natural and synthetic aluminosilicate glasses to classify different cases (see Table 3).

Table 3.

Some HEs are predominantly incorporated into the glass network as oxyanions with coordination numbers of 3 (As^{3+}, Sb^{3+}) and 4 (Mo^{6+}, V^{5+}). Increasingly oxidising conditions (and/or glass basicity) tend to stabilise complexes, such as $[Mo^{6+}O_4]^{2-}$, $[V^{5+}O_4]^{3-}$ or $[Cr^{6+}O_4]^{2-}$, which are not connected to the aluminosilicate glass tetrahedral network (Choi et al., 2000; Calas et al., 2003; Mallmann and O'Neill, 2009). In contrast, Sb undergoes complexation into the rings of four $[Sb^{3+}O_3]^{3-}$ oxyanions. Furthermore, Sb becomes less stable as the oxygen fugacity and glass basicity increase due to the oxidation to Sb^{5+} and its subsequent incorporation into the glass as a six-fold coordinated complex (Mee et al., 2010; Miller et al., 2019). Under the same conditions, As exists in the form of oxyanions such as $[As^{3+}O_3]^{3-}$ and $[As^{5+}O_4]^{3-}$ (Yoshida et al., 2010; Maciag and Brenan, 2020).

Other HEs are allocated with low coordination numbers (between 2 and 4) and relatively short metal–oxygen distances, such as Pb^{2+}, Se^{6+}, Cu^+, Zn^{2+}, and Ni^{2+} (Holzheid and Lodders, 2001; Calas et al., 2002; Ramos et al., 1992; Kacem et al., 2017; Kado et al., 2020). They do not form complexes, and their polyhedra are well integrated into the glass network; however, increasing the HE concentration and/or glass basicity increase the oxygen coordination (Galoisy and Calas, 1993; Lee et al., 2000; Méar et al., 2007).

Even if with high oxygen coordination, Cr^{3+} and Ba^{2+} do not act as glass network modifiers. In fact, Ba^{2+} usually serves as a charge compensator for Al^{3+} in the tetrahedral network (Mysen and Richet, 2018). Most commonly, Cr ions in aluminosilicate melts are octahedrally coordinated, and Cr^{3+}–Cr^{3+} dimers are formed at Cr_2O_3 concentrations exceeding 0.25% (Murata et al., 1997; Colson et al., 2000).

The allocation of HEs implies a competition between the crystals and the melt in terms of element dissolution. Thus, the preference of a given HE for a crystalline or amorphous phase can be predicted by performing a literature analysis on the partitioning of trace elements.

The concentration of a given element depends on its intrinsic properties, the properties of the host materials (crystals and melt), and the thermochemical conditions (Karato, 2016). Most geochemical studies focus on the partitioning of trace elements, generally at concentrations of less than 0.1 wt.%, to ensure that these elements have a negligible influence on physical/chemical processes (e.g. partial melting). Largely controlled by the difference in the excess free energy of a given element in co-existing materials, the preference of a trace element for a particular phase can be expressed by the partition coefficient that is equal to the ratio between the concentrations of a given element in two materials (Blundy and Wood, 2003; Karato, 2016). Although no studies exclusively devoted to silicate ceramics have been conducted, relevant data can be obtained from natural systems, in which crystals coexist with the melt. The average partition coefficients of various trace elements derived from the values listed in the Geochemical Earth Reference Model (GERM) database are shown in Figure 9 (GERM, 2021).
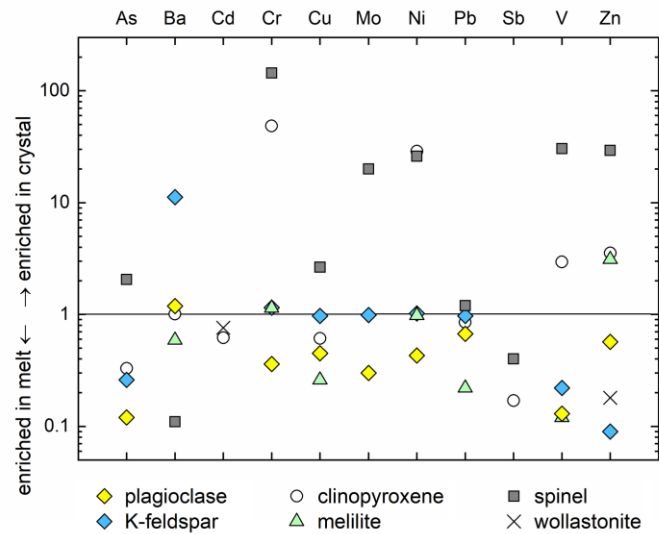
Figure 9.

Despite the high variability of the data presented in Figure 9, for each trace element in equilibrium with the crystalline phase and melt, it is possible to identify elements that preferentially enrich the crystalline phase and those that enrich the melt. For instance, the plagioclase/melt and K-feldspar/melt partitioning coefficients indicate that only Ba, and to a lesser extent, Cr (in the second system) enrich the crystalline phases. Cu, Mo, Ni, and Pb elements exhibit no partitioning preference in the K-feldspar/melt system. The melilite/melt partitioning data reveal that all the considered trace elements preferentially enrich the melt, except for Zn and Cr elements. No evidence of partitioning preference is observed for Ni in the melilite/melt system. In contrast to the above-mentioned systems, the partitioning coefficients obtained for the spinel/melt system clearly indicate that most HEs (in the following order of preference: Cr, V, Zn, Ni, Mo, Cu, As, and Pb) enrich the crystalline phase. Only Ba ions, which are too large to be hosted by the spinel lattice, and Sb enrich the melt. The most variable situation is represented by the clinopyroxene/melt partitioning data. Indeed, Cr, Zn, Ni,

and V elements enrich the crystalline phase, while Sb, As, Cu, and Cd enrich the melt. No preferences for Pb and Ba elements are observed for this crystal/melt system.

Based on the HE preferences determined for crystal and melt systems, it is possible to predict a possible allocation of these elements within the crystal lattices of the constituent phases or the vitreous phases of ceramic products. Similar to the previous example, Ba can enrich the crystal structures of the alkali feldspar and plagioclase phases during the firing transformations of largely recrystallised products (Figures 6b and c). Furthermore, in the firing temperature window determined for the porous tiles and bricks with high Ca and Mg contents (Figure 6b), Cr, Zn, Ni, and V elements can enrich the clinopyroxene crystal structure, and Zn the melilite phase.

Although we did not include chlorine in our review, it would be an oversimplification to avoid mentioning the effects related to the presence of Cl species in secondary raw materials. In addition to a variable quantity of HEs, a considerable amount of chlorine is usually present in bottom ash and fly ash (BA and FA, respectively) as well as in the flue gas produced by the municipal solid waste incineration (MSWI) (Alam et al., 2020; Ma et al., 2020). Although the processes in waste-to-energy plants are different from those occurring during the formation of ceramic products at high temperatures, some analogies can be drawn from the large number of literature studies on the presence of chlorine in BA and FA due to MSWI. Apart from its harmful environmental effects, chlorine is detrimental to the MSWI process because of the material deposition and corrosion of both the incinerator chamber and tubes (Ma et al., 2020). Moreover, when BA is used as a secondary raw material in the building industry, chlorine severely affects concrete structures due to the corrosion of steel reinforcements (Lynn et al., 2016; Alam et al., 2020). Chlorine speciation and amount are significantly influenced by several factors, including the Cl source (mainly plastic for organic Cl and food MSW for inorganic Cl) and temperature regime (Alam et al., 2020; Li et al., 2020; Ma et al., 2020). For instance, organic chlorides begin to release HCl at relatively low temperatures ($200 < T < 360$ °C) and decompose completely at approximately 550 °C, while inorganic KCl and NaCl salts volatilise and partially transform to HCl at approximately 800 °C (McNeill et al., 1995; Zhu et al., 2008; Li et al., 2020). At approximately 600 °C, HCl oxidises to form highly corrosive Cl_2 gas,

which in turn may lead to the formation of toxic products (such as dioxins) and affect the partitioning of heavy metals with strong implications for the environmental equilibrium (Yasuhara et al., 2001; Ma et al. 2020). Most importantly, increasing the chlorine content (both organic and inorganic) and combustion temperature causes the formation of volatile heavy metal compounds (oxides, silicates, and chlorides of Pb, Cu, Cr, Zn) and promotes their transfer from BA to FA and flue gas (Chiang et al., 1997a; Chiang et al., 1997b; Wang et al., 1997; Liu et al., 2015). Heavy metal partitioning is further affected by the presence of alkaline metals (such as Na and K) and moisture in waste products (Wang et al., 1999). Hence, it can be concluded that the presence of chlorine in waste can substantially change the mobility of metals within the ceramic body and that it is necessary to exercise caution when considering case studies involving recycled wastes with significant chlorine amounts.

4. Discussion

This section is mainly devoted to the causes and specific conditions of successful (especially at high immobilisation efficiency and high HE amounts) or unsuccessful inertisation by ceramisation (at low immobilisation efficiency).

Arsenic is effectively stabilised in silicate ceramics fired below 1100 °C because the average ε_{As} value is very high for both largely unreacted and largely recrystallised products ($\varepsilon_{As av}$ = 995.089‰ with a variance of 0.053‰ over a population of 41 data points when largely vitrified ceramic products are not considered). However, largely vitrified ceramics exhibit a notably high dispersion of results ($\varepsilon_{As av}$ = 938.335‰ with a variance of 5.541‰ over a population of 10 data points). Apart from the three low efficiency cases (ε_{As} < 90%), successful inertisation was observed at the highest As amounts in the batch. This was achieved when biomass BA was added to brick clay fired at 950 °C (Terrones et al., 2020). In such a largely recrystallised body, 0.07% As_2O_3 resulted in ε_{As} > 99.9%. As was also stabilised in a silica-rich body fired at 1225 °C with the addition of waste enriched with Fe, P, and Zn (Little et al., 2008). These elements lower the formation temperature of the liquid phase, but do not break the tetrahedral framework, helping

29

to retain 0.014% As_2O_3 with ε_{As} = 99.7%. Meanwhile, low ε_{As} values imply that partial mobilisation occurred for the As traces (10–21 mg/kg^{-1}) present in waste and ceramic bodies. This was observed when titania slag solubilisation waste was added to red stoneware (Contreras et al., 2014) and when a ceramic batch was fabricated from coal FA with 10% metal finishing waste (Little et al., 2008). Note that HQ_{As} values higher than one were obtained for harbour sludge (Alonso-Santurde et al., 2008), FA (Ponsot et al., 2015), metallurgical waste (electric arc furnace slag; Bantsis et al., 2011), and foundry sand (Alonso–Santurde et al., 2010). These cases included largely vitrified bodies with the highest firing temperatures in the dataset (1150–1225 °C), recrystallised product fired at a high temperature of 1000 °C, and largely unreacted products fired at a high temperature of 1020 °C. However, not all samples fired at high temperatures exhibited low immobilisation efficiency. The As mobilisation enhancement mechanism likely involved the As incorporation into the melt due to the low partition coefficients of As-containing species (Fig. 9 and relative discussion), and for $[As^{3+}O_3]^{3-}$ and $[As^{5+}O_4]^{3-}$ complexes. The batches with low ε_{As} are characterised by relatively low silica amounts as compared with those of alumina and oxides of iron, alkali-earth elements, and alkali elements. This leads to the formation of a rather basic melt, which is less polymerised and may facilitate As oxidation, and an easier release of arsenate complexes with respect to arsenite ones. Although crystal/melt partitioning data suggest that As is partitioned to a spinel-type crystalline phase, the related immobilisation efficiencies indicate that this HE preferentially enrich the melts of equilibrated clinopyroxene, K-feldspar, and plagioclase crystal/melt systems.

Barium is immobilised in silicate ceramics with very high efficiency ($\varepsilon_{Ba av}$ = 997.929‰ with a variance of 0.096‰ over a population of 64 data points) that corresponds to low HQ_{Ba} values (not exceeding 0.25) regardless of the body composition. This also occurred at high firing temperatures (1150–1350 °C) and large amounts of BaO (2–4%) in the batch (Bernardo et al., 2006; Mymrin et al., 2019). A single case of a much lower immobilisation efficiency was observed for a waste system composed of drilling mud and barite (Pinheiro et al., 2013). If this case is considered an outlier, the immobilisation efficiency of Ba is statistically comparable to that of Ni (the best case of HE immobilisation within ceramic products). Although the BaO concentration in a porcelain stoneware body was not particularly high (0.13 wt.%), firing was performed at 1240 °C, the temperature at which the

thermal decomposition of Ba sulphate had already occurred. The high Ba immobilisation efficiency in all the studied ceramic products is related to the following two factors. The first factor is the preserved amount (albeit in variable proportions) of plagioclase and K-feldspar (according to the crystal/melt partitioning data, Ba enriches the crystalline phases of the systems containing large feldspar and plagioclase contents). Second, the presence of the Al^{3+}, which needs a charge compensation, implies that Ba^{2+} ions are connected to the tetrahedral aluminosilicate glass framework.

Cadmium appears to be successfully incorporated into all types of silicate ceramics (ε_{Cdav} = 988.680‰ with a variance of 1.816‰ over a population of 17 data points); however, the interpretation of its high immobilisation efficiency suffers from data scarcity. The average Cd immobilisation efficiency can be even higher (ε_{Cdav} = 999.328‰ with a variance of 0.002‰ over a population of 16 data points), excluding a single outlier, although this result is based on a limited number of data points. It is noteworthy that the obtained dataset includes relatively high CdO concentrations: 4.05% CdS added to Ca–Na aluminosilicate glass (Sobieska et al., 2019) and 0.25% Cd nitrate introduced into a silica-rich body (Sharifikolouei et al., 2020). The lowest ε_{Cd} value has been obtained for a largely unreacted body fired at 850 °C (Quijorna et al., 2011), and it represents the only case with $HQ_{Cd} > 1$. However, a very small amount of Cd^{2+} ions was found in one of the four samples processed under the same conditions for liquid/solid ratio equals to 10.

Chromium was retained with high immobilisation efficiency, except for three cases out of 76 (ε_{Crav} = 997.239‰ with a variance of 0.028‰). Cr can enrich many crystalline phases (e.g. spinel, clinopyroxene, K-feldspar, and melilite) that are in equilibrium with the melt, which should theoretically lead to high leaching resistance and thus high immobilisation efficiency of the material. The average ε_{Cr} values vary slightly from the magnitudes obtained for largely unreacted bodies (99.9±0.1%) to those of largely recrystallised (99.6±0.1%) and largely vitrified (99.8±0.1%) products. This dataset includes Cr_2O_3 concentrations as high as 4.9% (Garcia-Valles et al., 2007) and 7.2% (Tang et al., 2019). The three cases, in which ε_{Cr} was approximately 97–98%, corresponded to low Cr_2O_3 concentrations of 0.01–0.02% and $HQ_{Cr} > 1$. Contreras et al. (2014) used red stoneware as a waste acceptor that contained a high amount of Cr (900 mg·kg^{-1}), which was partially lost during firing at 1150 °C. The other two cases included

31

largely recrystallised products that were fired at low temperatures (Quijorna et al., 2011). The oxidation of Cr^{3+} resulting in the formation of $[Cr^{6+}O_4]^{2-}$ complexes is a likely cause of Cr mobilisation. This phenomenon is well known in the field of silicate ceramics (Dondi et al., 1997; Abreu and Toffoli, 2009) and can be enhanced by lowering the firing temperature and increasing the CaO content.

Copper: Although the obtained crystal/melt partitioning data indicate that Cu can enrich crystalline phases (spinel and partially K-feldspar), it is efficiently immobilised in all ceramic products (ε_{Cuav} = 997.955‰ on average with a variance of 0.053‰ over a population of 52 data points). Cu is immobilised with ε_{Cu} ~99.9% in all largely unreacted and largely recrystallised bodies at firing temperatures below 1150 °C. A lower immobilisation efficiency as compared with those of the former two ceramic types was observed for largely vitrified products (951‰ < ε_{Cuav} < 1000‰) without crystalline spinel or K-feldspar phases. They included ceramic bodies that were fired at high temperatures (1200–1225 °C) and contained metal finishing waste with a tiny amount of Cu (Little et al., 2008) or electroplating sludge with 25% CuO (Tang et al., 2019). Although Cu leaching is enhanced at higher firing temperatures, as shown by Tang et al. (2019), other samples (such as porcelain stoneware) fired at approximately 1200 °C retained almost all the original Cu species (Schabbach et al., 2012). In the experiments performed by Little et al. (2008), the addition of waste rich in Fe, P, and Zn elements considerably reduced the Cu immobilisation efficiency. Interestingly, the same addition stabilised As species. The Cu mobilisation observed after firing at high temperatures can be explained by the oxidation to Cu^{2+} ions promoted by the high melt basicity or, in the case of high Cu contents, by the weaker Cu^+–O bonds at larger oxygen coordination numbers.

Lead can be successfully immobilised in silicate ceramics with a high efficiency comparable to that of Ba regardless of the batch composition (ε_{Pbav} = 995.630‰ with a variance of 0.205‰ over a population of 33 data points). This result was achieved for all batches with PbO contents over 0.1%, including concentrations as high as 3.3% (Sharifikolouei et al., 2020), 1.3% (Dondi et al., 2009), and 0.96% (Raimondo et al., 2007). The lowest immobilisation efficiency values (92 < ε_{Pb} <99%) were obtained in four cases involving low PbO amounts (0.003–0.007 wt.%) with largely unreacted bodies (Alonso-Santurde et al., 2011) as well as red stoneware containing titania slag waste (Contreras et al., 2014) and a largely recrystallised

product (Quijorna et al., 2011). Such low ε_{Pb} values correspond to HQ_{Pb} magnitudes higher than unity for largely unreacted and recrystallised bodies, including examples with ε_{Pb} > 99.9% coupled with HQ_{Pb} > 1 due to the high concentration of Pb in the starting batch (0.5–0.7 wt.%, Quijorna et al., 2011). Although the presence of Pb-bearing feldspars has been documented in the literature (Benna et al., 1996), the crystal/melt partitioning coefficient of Pb in feldspars does not show any evidence of the preferential Pb enrichment of the crystalline or melt phase.

Molybdenum stabilisation in silicate ceramics is challenging (ε_{Moav} = 763.960‰ with a variance of 61.851‰ over a population of 32 data points) because most samples exhibit low Mo immobilisation efficiency (12 < ε_{Mo} < 95%). In addition, data are available only for very low MoO_3 contents in the batch (below 0.007%) and firing temperatures up to 1050 °C; as a result, the obtained HQ_{Mo} is always greater than unity, which increases the degree of experimental uncertainty during the analysis of ceramic bodies and leachate. Furthermore, no information on the Mo stabilisation in largely vitrified ceramics is available. Despite these limitations, the lowest Mo immobilisation efficiency (ε_{Mo} < 70%) was observed for largely unreacted bodies (ε_{Mo} = 70±30%). In contrast, largely recrystallised bodies mostly exhibited ε_{Mo} values between 70% and 95% (ε_{Mo} = 83±14%). In all cases, full Mo stabilisation was possible (Quijorna et al., 2011 and 2012; Coronado et al., 2015). The low Mo immobilisation efficiency agrees well with the crystal/melt partitioning data (see section 3.2), according to which Mo enriches exclusively the crystalline phase with a spinel structure, such as magnetite (an inverse spinel with the composition $Fe^{2+}Fe^{3+}_2O_4$) in equilibrium with the corresponding melt (Karamanov et al., 2000). Meanwhile, even under favourable chemical and thermodynamic conditions, Mo has to compete with other HEs to be hosted in the spinel lattice. Indeed, Cr, Al, and Ti, the main elements that form solid solutions with magnetite, should be located in the spinel lattice prior to Mo exposure. Overall, the difficulties related to Mo stabilisation likely result from the formation of molybdates with a larger water solubility than that of the silicate components. The observed differences between largely unreacted and largely recrystallised bodies may be related to the presence of alkali and alkali-earth molybdates with different water solubilities.

33

Nickel was efficiently immobilised in silicate ceramics ($\varepsilon_{Ni\,av}$ = 999.047‰ with a variance of 0.004‰ over a population of 35 data points). This was achieved even at fairly small amounts of NiO: 0.66% (Garcia-Valles et al., 2007) and 0.16% (Quijorna et al., 2011). The lowest Ni immobilisation efficiency (ε_{Ni} = 99.0%) obtained for largely unreacted bodies fired at 850 °C (Quijorna et al., 2011) is consistent with a high hazard quotient (HQ_{Ni} > 1). The easy immobilisation of Ni is likely caused by its strong affinity for stable crystalline phases (such as pyroxene and spinel) and incorporation into the glass network at the $Ni^{2+}–O_4$ or $Ni^{2+}–O_5$ polyhedra stabilised by alkali and/or alkali earth elements.

Zinc is easily immobilised in silicate ceramics ($\varepsilon_{Zn\,av}$ = 998.854‰ with a variance of 0.006‰ over a population of 56 data points). Similar results were also obtained for high ZnO contents: up to ~1% in largely unreacted bodies (Cifrian et al., 2019), up to ~1.5% in largely recrystallised ceramics (Quijorna et al., 2011), and up to ~2.2% in largely vitrified products (Tan et al., 2012). Nevertheless, there are cases of almost total ceramic inertisation (with approximately ε_{Zn} > 99.7%) and slightly lower Zn immobilisation efficiency values (ε_{Zn} < 99.7%). In the latter examples, the lowest efficiency was obtained for the red stoneware case discussed earlier (Contreras et al., 2014) and two out of five largely recrystallised products investigated by Pérez-Villarejo et al. (2015), in which ε_{Zn} scaled approximately with the ZnO content. Zn can enrich the crystal lattices of spinel, clinopyroxene, and melilite in equilibrium with the melt or be stabilised in aluminosilicate glass where Zn^{2+} ions exist in the tetrahedral coordination with relatively short bond distances.

Antimony data include only two cases: Sb traces in a largely unreacted product (Alonso-Santurde et al., 2011) and 0.3–0.6% Sb_2O_5 in glass ceramics (Bernardo et al., 2006). In both studies, the calculated ε_{Sb} values exceeded 99.9%. The inertisation efficiencies of HEs which preferentially occurr as oxyanions is similar for Sb, As, and Cr, but it is much lower for Mo. Nevertheless, the mobilised fraction of As or Cr can increase the hazard quotient above unity (with a comparable frequency in the dataset). At the moment, only a generic analogy of behavior can be grasped between the various oxyanions, since the literature does not provide specific indications on the valence of HE and on its possible change during firing of silicate

ceramics. Further studies are needed to establish which oxyanions are most stable under ceramic firing conditions, and the tendency to form their own crystalline phases.

5. Conclusions

The introduction of waste materials into silicate ceramics from the perspective of a full transition to a circular economy is complicated by the likely presence of HEs in secondary raw materials. In this study, a theoretical framework was developed and applied to (1) identify HEs that are problematic for ceramic production; (2) parameterise the degree of immobilisation of HEs after their incorporation into a ceramic matrix; (3) elucidate the reaction through which a given element can be immobilised in the ceramic matrix during firing; and (4) select successful and unsuccessful cases of waste recycling in silicate ceramics from the published literature studies.

As no regulations exist regarding the elements that can be considered hazardous in ceramic bodies, ceramic inertisation efficiency was estimated from the results of leaching tests conducted for silicate ceramics and limits established for landfilling inert wastes. The identified HEs (Ba, Zn, Cu, Cr, Mo, As, Pb, Ni, Sb, and Cd, in the increasing order of danger) were parameterised by three descriptors (*immobilisation efficiency*, *mobilised fraction*, and *hazard quotient*). It was found that ceramics must have a remarkably high immobilisation efficiency (often above 99.9% for HE concentrations greater than 1 wt.%).

The incorporation of HEs into ceramic products occurred both in the lattice of crystalline phases and glassy networks of vitreous phases at the expense of other major and minor elements constituting ceramic bodies. The later were classified into *largely vitrified*, *largely recrystallised*, and *largely unreacted* bodies based on the phase transformations occurring during heat treatment.

This literature survey suggests an overall benefit of waste recycling in silicate ceramics that can immobilise HEs with a remarkably high efficiency. This is particularly true for Ba, Zn, Ni, and Cd elements, which are efficiently immobilised in all instances, including different ceramic bodies and firing

35

conditions. Nonetheless, the introduction of HEs into ceramic bodies may also conceal pitfalls that must be identified and mitigated. The literature reports several cases, in which the hazard quotient was higher than the limit established for inert materials. They involved Mo (100% of all cases), Cr (31% of all cases), and Pb (35% of all cases) HEs. Such unsatisfactory HE immobilisation can be attributed to the use of largely unreacted and recrystallised ceramic types. Furthermore, for several As (28% of cases) and Cu (12% of cases) samples, the hazard quotient exceeded unity. It must be emphasised that the literature data do not provide adequate statistics to draw conclusions regarding the mobility of HEs under variable conditions. To obtain a complete picture describing the effect of the ceramic body type and firing schedule on HE immobilisation, further studies are required.

The formation of oxy-anionic complexes that produce their own phases or are not linked to the tetrahedral aluminosilicate glass framework, such as $[Cr^{6+}O_4]^{2-}$, $[Mo^{6+}O_4]^{2-}$, and $[As^{3+}O_3]^{3-}$, is the most likely mechanism of the enhanced HE mobilisation. Pb and Cu can be preferentially partitioned to the melt because of their low coordination numbers and relatively long oxygen bond distances (Pb^{2+} [3] 2.25 Å; Cu^+ [2] 1.84 Å). Nevertheless, Cr, Pb, and Cu elements were effectively immobilised by silicate ceramics, and their average immobilisation efficiency was higher than 99.6%. In all cases, the comprehension of the actual mechanism of HE immobilisation in silicate ceramics deserves to be the subject of future research. Above all, understanding how different the behavior is between widely crystallised, glassy or unreacted systems can pave the way for a real engineering of waste recycling.

The major elements of concern identified in this work include As and Mo. In particular, the stabilisation of Mo in silicate ceramics appears to be challenging and totally ineffective in some cases. Hence, it is necessary to develop a special inertisation strategy for these two HEs that is based on the properties of a ceramic matrix and its constituent phases.

Declaration of Competing Interest

☒ The authors declare that they have no known competing financial interests or personal relationships that could have appeared to influence the work reported in this paper.

☐The authors declare the following financial interests/personal relationships which may be considered as potential competing interests:

References

Abreu, M. A., & Toffoli, S. M. (2009). Characterization of a chromium-rich tannery waste and its potential use in ceramics. Ceramics International, 35(6), 2225-2234.

Akinshipe, O., & Kornelius, G. (2017). Chemical and thermodynamic processes in clay brick firing technologies and assosciated atmospheric emissions metrics-a review. Journal of Pollution Effects & Control, 5, 190 (12 p.).

Alam, Q., Lazaro, A., Schollbach, K., & Brouwers, H. J. H. (2020). Chemical speciation, distribution and leaching behavior of chlorides from municipal solid waste incineration bottom ash. Chemosphere, 241, 124985.

Al-Abed, S.R., Jegadeesan, G., Purandare, J., Allen, D. (2008). Leaching behavior of mineral processing waste: Comparison of batch and column investigations. Journal of Hazardous Materials 153, 1088–1092.

Al-Fakih, A., Mohammed, B. S., Liew, M. S., & Nikbakht, E. (2019). Incorporation of waste materials in the manufacture of masonry bricks: An update review. Journal of Building Engineering, 21, 37-54.

Allali, D., Bouhemadou, A., Muhammad Abud Al Safi, E., Bin-Omran, S., Chegaar, M., Khenata, R., & Reshak A.H. (2014). Electronic and optical properties of the SiB_2O_4 (B=Mg, Zn, and Cd) spinel oxides: An ab initio study with the Tran–Blaha-modified Becke–Johnson density functional. Physica B: Condensed Matter, 443, 24-34.

Alonso-Santurde, R., Andrés, A., Viguri, J. R., Raimondo, M., Guarini, G., Zanelli, C., & Dondi, M. (2011). Technological behaviour and recycling potential of spent foundry sands in clay bricks. Journal of Environmental Management, 92(3), 994-1002.

Alonso-Santurde, R., Coz, A., Quijorna, N., Viguri, J. R., & Andrés, A. (2010). Valorization of Foundry Sand in Clay Bricks at Industrial Scale: Environmental Behavior of Clay− Sand Mixtures. Journal of Industrial Ecology, 14(2), 217-230.

Alonso-Santurde, R., Romero, M., Rincón López, J. M., Viguri, J., & Andres, A. (2008). Leaching behaviour of sintered contaminated marine sediments. Fresenius Environmental Bulletin, 17, 1736-1743

Andreola, F., Barbieri, L., Lancellotti, I., Leonelli, C., & Manfredini, T. (2016). Recycling of industrial wastes in ceramic manufacturing: State of art and glass case studies. Ceramics International, 42(12), 13333-13338.

Andreola, F., Barbieri, L., Soares, B. Q., Karamanov, A., Schabbach, L. M., Bernardin, A. M., & Pich, C. T. (2019). Toxicological analysis of ceramic building materials–Tiles and glasses–Obtained from post-treated bottom ashes. Waste Management, 98, 50-57.

Andreola, F., Lancellotti, I., Manfredini, T., & Barbieri, L. (2020). The circular economy of agro and post-consumer residues as raw materials for sustainable ceramics. International Journal of Applied Ceramic Technology, 17(1), 22-31.

Ardit, M., Dondi, M., Merlini, M., & Cruciani, G. (2012a). Melilite-type and melilite-related compounds: structural variations along the join $Sr_{2-x}Ba_xMgSi_2O_7$ (0≤x≤2) and high-pressure behavior of the two end-members" Physics and Chemistry of Minerals, 39, 199-211.

Ardit, M., Cruciani, G., & Dondi, M. (2012b). Local structural relaxation around Co^{2+} along the hardystonite–Co-åkermanite melilite solid solution. Physics and Chemistry of Minerals, 39, 713-723.

Ballato, P., Cruciani, G., Dalconi, M. C., Fabbri, B., & Macchiarola, M. (2005). Mineralogical study of historical bricks from the Great Palace of the Byzantine Emperors in Istanbul based on powder X-ray diffraction data. European Journal of Mineralogy, 17(5), 777-784.

Bantsis, G., Sikalidis, C., Betsiou, M., Yioultsis, T., & Bourliva, A. (2011). Ceramic building materials for electromagnetic interference shielding using metallurgical slags. Advances in Applied Ceramics, 110(4), 233-237.

Baur, W.H. (1974). The geometry of polyhedral distortions. Predictive relationships for the phosphate group. Acta Crystallographica B, 30, 1195-1215.

Bellotto, M., Gualtieri, A., Artioli, G., & Clark, S. M. (1995). Kinetic study of the kaolinite-mullite reaction sequence. Part I: kaolinite dehydroxylation. Physics and chemistry of minerals, 22(4), 207-217.

Benna, P., Tribaudino, M., & Bruno, E. (1996). The structure of ordered and disordered lead feldspar ($PbAl_2Si_2O_8$). American Mineralogist, 81, 1337-1343.

Bernardo, E., Bonomo, E., & Dattoli, A. (2010). Optimisation of sintered glass–ceramics from an industrial waste glass. Ceramics International, 36(5), 1675-1680.

Bernardo, E., Varrasso, M., Cadamuro, F., & Hreglich, S. (2006). Vitrification of wastes and preparation of chemically stable sintered glass-ceramic products. Journal of Non-Crystalline Solids, 352(38-39), 4017-4023.

Bernasconi, A., Dapiaggi, M., Bowron, D., Ceola, S., & Maurina, S. (2016). Aluminosilicate-based glasses structural investigation by high-energy X-ray diffraction. Journal of Materials Science, 51(19), 8845-8860.

Bernasconi, A., Marinoni, N., Pavese, A., Francescon, F., & Young, K. (2014). Feldspar and firing cycle effects on the evolution of sanitary-ware vitreous body. Ceramics International, 40(5), 6389-6398.

Bosi, F., Skogby, H., Fregola, R.A., & Hålenius, U. (2016). Crystal chemistry of spinels in the system $MgAl_2O_4$-MgV_2O_4-Mg_2VO_4. American Mineralogist, 101, 580-586.

Blundy J.D. & Wood, B.J. (2003) Partitioning of trace elements between crystals and melts. Earth and Planetary Science Letters, 210, 383-397.

Calas, G., Cormier, L., Galoisy, L., & Jollivet, P. (2002). Structure–property relationships in multicomponent oxide glasses. Comptes Rendus Chimie, 5(12), 831-843.

Calas, G., Le Grand, M., Galoisy, L., & Ghaleb, D. (2003). Structural role of molybdenum in nuclear glasses: an EXAFS study. Journal of Nuclear Materials, 322, 15-20.

Carty, W. M., & Senapati, U. (1998). Porcelain—raw materials, processing, phase evolution, and mechanical behavior. Journal of the American Ceramic Society, 81(1), 3-20.

Chiang, K. Y., Wang, K. S., & Lin, F. L. (1997a). The effect of inorganic chloride on the partitioning and speciation of heavy metals during a simulated municipal solid waste incineration process. Toxicological & Environmental Chemistry, 64(1-4), 109-126.

Chiang, K. Y., Wang, K. S., Lin, F. L., & Chu, W. T. (1997b). Chloride effects on the speciation and partitioning of heavy metal during the municipal solid waste incineration process. Science of the total environment, 203(2), 129-140.

Choi, Y. G., Kim, K. H., Han, Y. S., & Heo, J. (2000). Oxidation state and local coordination of chromium dopant in soda-lime-silicate and calcium-aluminate glasses. Chemical Physics Letters, 329(5-6), 370-376.Clark et al., 1969.

Cifrian, E., Coronado, M., Quijorna, N., Alonso-Santurde, R., & Andrés, A. (2019). Waelz slag-based construction ceramics: effect of the trial scale on technological and environmental properties. Journal of Material Cycles and Waste Management, 21(6), 1437-1448.

Clark, J.R., Appleman, D.E., & Papike, J.J. (1969). Crystal-chemical characterization of clinopyroxenes based on eight new structure refinements. Mineralogical Society of America: Special Papers, 2, 31-50.

Colson, R. O., Colson, M. C., Nermoe, M. K., Floden, A. M., & Hendrickson, T. R. (2000). Effects of aluminum on Cr dimerization in silicate melts and implications for Cr partitioning and redox equilibria. Geochimica et Cosmochimica Acta, 64(3), 527-543.

Conte, S., Zanelli, C., Ardit, M., Cruciani, G., & Dondi, M. (2020). Phase evolution during reactive sintering by viscous flow: Disclosing the inner workings in porcelain stoneware firing. Journal of the European Ceramic Society, 40, 1738-1752.

Contreras, M., Martín, M. I., Gázquez, M. J., Romero, M., & Bolívar, J. P. (2014). Valorisation of ilmenite mud waste in the manufacture of commercial ceramic. Construction and Building Materials, 72, 31-40.

Coronado, M., Blanco, T., Quijorna, N., Alonso-Santurde, R., & Andrés, A. (2015). Types of waste, properties and durability of toxic waste-based fired masonry bricks. In: Eco-Efficient Masonry Bricks and Blocks, pp. 129-188, Woodhead Publishing.

Coronado, M., Segadães, A. M., & Andrés, A. (2015). Using mixture design of experiments to assess the environmental impact of clay-based structural ceramics containing foundry wastes. Journal of hazardous materials, 299, 529-539.

Council Decision of 19 December 2002 establishing criteria and procedures for the acceptance of waste at landfills pursuant to Article 16 of and Annex II to Directive 1999/31/EC (2003/33/EC)

Cultrone, G., Rodriguez-Navarro, C., Sebastian, E., Cazalla, O., & De La Torre, M. J. (2001). Carbonate and silicate phase reactions during ceramic firing. European Journal of Mineralogy, 13(3), 621-634.

Cultrone, G., Sebastian, E., & De La Torre, M. J. (2005). Mineralogical and physical behaviour of solid bricks with additives. Construction and Building Materials, 19, 39–48.

Djordjevic, J., Dondur, V., Dimitrijevic, R., & Kremenovic, A. (2001). Structural investigations of celsian glass derived from Ba-LTA zeolite. Physical Chemistry Chemical Physics, 3, 1560-1565.

Donald, I. W. (2010). Waste immobilization in glass and ceramic based hosts: radioactive, toxic and hazardous wastes. John Wiley & Sons.

Donatello, S., Tyrer, M., Cheeseman, C.R. (2010). EU landfill waste acceptance criteria and EU Hazardous Waste Directive compliance testing of incinerated sewage sludge ash. Waste Management 30, 63–71.

Dondi, M., Cappelletti, P., D'Amore, M., De Gennaro, R., Graziano, S. F., Langella, A., Raimondo, M. & Zanelli, C. (2016). Lightweight aggregates from waste materials: Reappraisal of expansion behavior and prediction schemes for bloating. Construction and Building Materials, 127, 394-409.

Dondi, M., Ercolani, G., Fabbri, B., & Marsigli, M. (1998). An approach to the chemistry of pyroxenes formed during the firing of Ca-rich silicate ceramics. Clay Minerals, 33(3), 443-452.

Dondi, M., Ercolani, G., Fabbri, B., & Marsigli, M. (1999a). Chemical Composition of Melilite Formed during the Firing of Carbonate-Rich and Iron-Containing Ceramic Bodies. Journal of the American Ceramic Society, 82(2), 465-468.

Dondi, M., Ercolani, G., Guarini, G., & Raimondo, M. (1999c). Microstruttura delle piastrelle ceramiche a supporto poroso. Influenza della composizione dell'impasto e della tecnologia di processo. Ceramica Informazione, 392, 849-857.

Dondi, M., Ercolani, G., Guarini, G., & Raimondo, M. (2002). Orimulsion fly ash in clay bricks—part 1: composition and thermal behaviour of ash. Journal of the European Ceramic Society, 22, 11, 1729-1735.

Dondi, M., Fabbri, B., & Mingazzini, C. (1997). Mobilisation of Chromium and Vanadium during firing of structural clay products. Ziegelindustrie *International*, *50*(10), 685-696.

Dondi, M., Guarini, G., & Raimondo, M. (1999b). Trends in the formation of crystalline and amorphous phases during the firing of clay bricks. Tile & brick international, 15(3), 176-178.

Dondi, M., Guarini, G., Raimondo, M., & Zanelli, C. (2009). Recycling PC and TV waste glass in clay bricks and roof tiles. Waste management, 29(6), 1945-1951.

Dondi, M., Marsigli, M., & Fabbri, B. (1997). Recycling of industrial and urban wastes in brick production- A review. Tile & Brick International, 13(3), 218-225.

Du, J.M., Zeng, H.Y., Song, L.J., Dong, Z.C., Ma, H.W., Guo, G.C., & Huang, J.S. (2003). Synthesis and structure of a new polymorph $Ba_2CuSi_2O_7$. Jiegou Huaxue, 22, 33-36.

Dunham, A. C. (1992). Developments in industrial mineralogy: I. The mineralogy of brick-making. Proceedings of the Yorkshire Geological Society, 49, 95.

Ewing, R. C., & Lutze, W. (1991). High-level nuclear waste immobilization with ceramics. Ceramics International, 17(5), 287-293.

Farges, F., Siewert, R., Brown Jr, G. E., Guesdon, A., & Morin, G. (2006). Structural environments around molybdenum in silicate glasses and melts. I. Influence of composition and oxygen fugacity on the local structure of molybdenum. The Canadian Mineralogist, 44, 731-753.

Fernández-Pereira, C., De La Casa, J. A., Gómez-Barea, A., Arroyo, F., Leiva, C., & Luna, Y. (2011). Application of biomass gasification fly ash for brick manufacturing. Fuel, 90(1), 220-232.

Ferrari, G., & Zannini, P. (2017). VOCs monitoring of new materials for ceramic tiles decoration: GC–MS analysis of emissions from common vehicles and inkjet inks during firing in laboratory. Boletín de la Sociedad Española de Cerámica y Vidrio, 56(5), 226-236.

Fischer, R.X. & Schneider, H. (2000). Crystal structure of Cr-mullite. American Mineralogist, 85, 1175-1179.

Fortes, A.D. (2015). Crystal structures of spinel-type Na_2MoO_4 and Na_2WO_4 revisited using neutron powder diffraction. Acta Crystallographica E, 71, 592-596.

Galoisy, L., & Calas, G. (1993). Structural environment of nickel in silicate glass/melt systems: Part 1. Spectroscopic determination of coordination states. Geochimica et Cosmochimica Acta, 57, 3613-3626.

Galvín, A.P., Ayuso, J., Jiménez, J.R., Agrela, F. (2012). Comparison of batch leaching tests and influence of pH on the release of metals from construction and demolition wastes. Waste Management 32, 88–95.

Garcia-Valles, M., Avila, G., Martinez, S., Terradas, R., & Nogués, J. M. (2007). Heavy metal-rich wastes sequester in mineral phases through a glass–ceramic process. Chemosphere, 68(10), 1946-1953.

GERM (2020). Partition coefficient Database, https://earthref.org, last accessed in December 2020).

González-Corrochano, B., Alonso-Azcárate, J., Rodríguez, L., Pérez Lorenzo, A., Fernández Torío, M., Tejado Ramos, J. J., Corvinos, M. D. & Muro, C. (2018). Effect heating dwell time has on the retention of heavy metals in the structure of lightweight aggregates manufactured from wastes. Environmental technology, 39(19), 2511-2523.

Golge, O., Hepsag, F., & Kabak, B. (2018). Health risk assessment of selected pesticide residues in green pepper and cucumber. Food and Chemical Toxicology, 121, 51-64.

Gualtieri, A. F. (2007). Thermal behavior of the raw materials forming porcelain stoneware mixtures by combined optical and in situ x-ray dilatometry. Journal of the American Ceramic Society, 90(4), 1222-1231.

Gualtieri, A., & Bellotto, M. (1998). Modelling the structure of the metastable phases in the reaction sequence kaolinite-mullite by X-ray scattering experiments. Physics and Chemistry of Minerals, 25(6), 442-452.

Haiying, Z., Youcai, Z., & Jingyu, Q. (2007). Study on use of MSWI fly ash in ceramic tile. Journal of Hazardous Materials, 141(1), 106-114.

Haiying, Z., Youcai, Z., & Jingyu, Q. (2011). Utilization of municipal solid waste incineration (MSWI) fly ash in ceramic brick: product characterization and environmental toxicity. Waste Management, 31(2), 331-341.

Heimann, R. B., & Maggetti, M. (2019). The struggle between thermodynamics and kinetics: Phase evolution of ancient and historical ceramics. The contribution of mineralogy to cultural heritage, 20, 233-281.

Holzheid, A., & Lodders, K. (2001). Solubility of copper in silicate melts as function of oxygen and sulfur fugacities, temperature, and silicate composition. Geochimica et Cosmochimica Acta, 65, 1933-1951.

Hoppe R. (1979). Effective coordination numbers (ECoN) and mean fictive ionic radii (MEFIR). Zeitschrift für Kristallographie, 150, 23-52.

Hossain, S. S., & Roy, P. K. (2020). Sustainable ceramics derived from solid wastes: A review. Journal of Asian Ceramic Societies, 8(4), 984-1009.

ISO 6486-1:2019, Ceramic ware, glass ceramic ware and glass dinnerware in contact with food — Release of lead and cadmium; and ISO 6486-2:1999, Ceramic ware, glass-ceramic ware and glass dinnerware in contact with food — Release of lead and cadmium — Part 2: Permissible limits.

ISO/WD 10545-15. Ceramic tiles — Part 15: Determination of lead and cadmium provided by glazed tiles.

Jarrige, J. & Mexmain, J. (1990). Etude du manganite de cuivre $CuMn_2O_4$ cubique et quadratique. Bulletin de la Société Chimique de France, 127, 628-634.

Kacem, I. B., Gautron, L., Coillot, D., & Neuville, D. R. (2017). Structure and properties of lead silicate glasses and melts. Chemical Geology, 461, 104-114.

Kado, R., Kishi, T., Lelong, G., Galoisy, L., Matsumura, D., Calas, G., & Yano, T. (2020). Structural significance of nickel sites in aluminosilicate glasses. Journal of Non-Crystalline Solids, 539, 120070.

Kaiser, J. W. & Jeitschko, W. (2002). Crystal structure of the new barium zinc silicate $Ba_2ZnSi_2O_7$. Zeitschrift für Kristallographie - New Crystal Structures, 217, 25-26.

Kalmykova, Y., Sadagopan, M., & Rosado, L. (2018). Circular economy–From review of theories and practices to development of implementation tools. Resources, conservation and recycling, 135, 190-201.

Kamiya, K., Okasaka, K., Wada, M., Nasu, H., & Yoko, T. (1992). Extended X-ray absorption fine structure (EXAFS) study on the local environment around copper in low thermal expansion copper aluminosilicate glasses. Journal of the American Ceramic Society, 75, 477-478.

Karamanov, A., Pisciella, P., Cantalini, C., & Pelino, M. (2000). Influence of Fe3+/Fe2+ ratio on the crystallization of iron rich-glasses made with industrial wastes, Journal of the American Ceramic Society, 83, 2153-2157.

Karayannis, V. G., Karapanagioti, H. K., Domopoulou, A. E., & Komilis, D. P. (2017). Stabilization/solidification of hazardous metals from solid wastes into ceramics. Waste and Biomass Valorization, 8(5), 1863-1874.

Karato, S.-I. (2016) Physical basis of trace element partitioning: A review. American Mineralogist, 101, 2577-2593.

Karnis, A., & Gautron, L. (2009). Promising immobilization of cadmium and lead inside Ca-rich glass-ceramics. International Journal of Geological and Environmental Engineering, 3, 100-103.

Kim, M., Ha, M.G., Um, W., Kim, H.G., Hong, K.S. (2020). Relationship between leaching behavior and glass structure of calcium-aluminoborate waste glasses with various La_2O_3 contents. Journal of Nuclear Materials 539, 152331.

Kinnunen, P., Ismailov, A., Solismaa, S., Sreenivasan, H., Räisänen, M. L., Levänen, E., & Illikainen, M. (2018). Recycling mine tailings in chemically bonded ceramics–a review. Journal of Cleaner Production, 174, 634-649.

Kiselev, E.A., Proskurnina, N.V., Voronin, V.I., & Cherepanov, V.A. (2007). Phase equilibria and crystal structures of phases in the La - Fe - Ni - O system at 1370 K in air. Neorganicheskie Materialy, 43, 209-217.

Krüger, O., Kalbe, U., Berger, W., Simon, F.-G., López Meza, S. (2012). Leaching experiments on the release of heavy metals and PAH from soil and waste materials. Journal of Hazardous Materials 207–208 (2012) 51–55.

Lee, W. E., Ojovan, M. I., Stennett, M. C., & Hyatt, N. C. (2006). Immobilisation of radioactive waste in glasses, glass composite materials and ceramics. Advances in Applied Ceramics, 105(1), 3-12.

Lee, J., Yano, T., Shibata, S., Nukui, A., & Yamane, M. (2000). EXAFS study on the local environment of Cu+ ions in glasses of the $Cu_2O–Na_2O–Al_2O_3–SiO_2$ system prepared by Cu^+/Na^+ ion exchange. Journal of non-crystalline solids, 277, 155-161.

Lenaz, D., Skogby, H., Princivalle, F. & Hålenius, U. (2004). Structural changes and valence states in the $MgCr_2O_4–FeCr_2O_4$ solid solution series. Physics and Chemistry of Minerals, 31, 633-642.

Li, W., Liu, D., Shen, D., Hu, L., Yao, J., & Long, Y. (2020). Migration of inorganic chlorine during thermal treatment of mineralized waste. Waste Management, 104, 207-212.

Little, M. R., Adell, V., Boccaccini, A. R., & Cheeseman, C. R. (2008). Production of novel ceramic materials from coal fly ash and metal finishing wastes. Resources, Conservation and Recycling, 52(11), 1329-1335.

Liu, J., Fu, J., Sun, S., Wang, Y., Xie, W., Huang, S., & Zhong, S. (2015). An experimental and thermodynamic equilibrium investigation of the Pb, Zn, Cr, Cu, Mn and Ni partitioning during sewage sludge incineration. Journal of Environmental Sciences, 35, 43-54.

Liu, T., Zhang, J., Wu, J., Liu, J., Li, C., Ning, T., & Lu, A. (2019). The utilization of electrical insulators waste and red mud for fabrication of partially vitrified ceramic materials with high porosity and high strength. Journal of cleaner production, 223, 790-800.

Loncnar, M., van der Sloot, H.A., Mladenovič, A., Zupančič, M., Kobal, L., Bukovec, P. (2016). Study of the leaching behaviour of ladle slags by means of leachingtests combined with geochemical modelling and mineralogical investigations. Journal of Hazardous Materials 317, 147–157.

Lu, X., Ning, X., Lee, P.H., Shih, K., Wang, F., Zeng, E.Y. (2017). Transformation of hazardous lead into lead ferrite ceramics: Crystal structures and their role in lead leaching. Journal of Hazardous Materials 336, 139–145.

Lu, X., Yang, J., Ning, X. A., Shih, K., Wang, F., & Chao, Y. (2019). Formation of lead ferrites for immobilizing hazardous lead into iron-rich ceramic matrix. Chemosphere, 214, 239-249.

Lynn, C. J., OBE, R. K. D., & Ghataora, G. S. (2016). Municipal incinerated bottom ash characteristics and potential for use as aggregate in concrete. Construction and Building Materials, 127, 504-517.

Ma, W., Wenga, T., Frandsen, F. J., Yan, B., & Chen, G. (2020). The fate of chlorine during MSW incineration: Vaporization, transformation, deposition, corrosion and remedies. Progress in Energy and Combustion Science, 76, 100789.

Maciag, B. J., & Brenan, J. M. (2020). Speciation of arsenic and antimony in basaltic magmas. Geochimica et Cosmochimica Acta, 276, 198-218.

Magalhães, J. M., Silva, J. E. D., Castro, F. P., & Labrincha, J. A. (2004). Effect of experimental variables on the inertization of galvanic sludges in clay-based ceramics. Journal of Hazardous Materials, 106, 139-147.

Malinovskii, Yu.A. (1984). The crystal structure of $Ba_2CuSi_2O_7$. Doklady Akademii Nauk SSSR, 278, 616-619.

Mallmann, G., & O'Neill, H. S. C. (2009). The crystal/melt partitioning of V during mantle melting as a function of oxygen fugacity compared with some other elements (Al, P, Ca, Sc, Ti, Cr, Fe, Ga, Y, Zr and Nb). Journal of Petrology, 50, 1765-1794.

Mao, L., Guo, H., & Zhang, W. (2018). Addition of waste glass for improving the immobilization of heavy metals during the use of electroplating sludge in the production of clay bricks. Construction and Building Materials, 163, 875-879.

Martínez-García, C., Eliche-Quesada, D., Pérez-Villarejo, L., Iglesias-Godino, F. J., & Corpas-Iglesias, F. A. (2012). Sludge valorization from wastewater treatment plant to its application on the ceramic industry. Journal of environmental management, 95, S343-S348.

McCloy, J. S., & Goel, A. (2017). Glass-ceramics for nuclear-waste immobilization. Mrs Bulletin, 42(3), 233-240.

McKeown, D. A., Gan, H., & Pegg, I. L. (2017). X-ray absorption and Raman spectroscopy studies of molybdenum environments in borosilicate waste glasses. Journal of Nuclear Materials, 488, 143-149.

McKeown, D. A., Muller, I. S., Matlack, K. S., & Pegg, I. L. (2002). X-ray absorption studies of vanadium valence and local environment in borosilicate waste glasses using vanadium sulfide, silicate, and oxide standards. Journal of non-crystalline solids, 298, 160-175.

McNeill, I. C., Memetea, L., & Cole, W. J. (1995). A study of the products of PVC thermal degradation. Polymer Degradation and Stability, 49(1), 181-191.

Méar, F. O., Yot, P. G., Kolobov, A. V., Ribes, M., Guimon, M. F., & Gonbeau, D. (2007). Local structure around lead, barium and strontium in waste cathode-ray tube glasses. Journal of non-crystalline solids, 353, 4640-4646.

Mee, M., Davies, B. C., Orman, R. G., Thomas, M. F., & Holland, D. (2010). Antimony and silicon environments in antimony silicate glasses. Journal of Solid State Chemistry, 183, 1925-1934.

Miller, L. A., O'Neill, H. S. C., Berry, A. J., & Glover, C. J. (2019). The oxidation state and coordination environment of antimony in silicate glasses. Chemical Geology, 524, 283-294.

Minguillón, M. C., Monfort, E., Querol, X., Alastuey, A., Celades, I., & Miró, J. V. (2009). Effect of ceramic industrial particulate emission control on key components of ambient PM10. Journal of Environmental Management, 90(8), 2558-2567.

Monfort, E., Celades López, I., Gomar Peiró, S., Rueda, F., & Martínez, J. (2011). Characterisation of acid pollutant emissions in ceramic tile manufacture. Boletín de la Sociedad Española de Cerámica y Vidrio, 50, 179-184.

Murata, T., Torisaka, M., Takebe, H., & Morinaga, K. (1997). Compositional dependence of the valency state of Cr ions in oxide glasses. Journal of Non-Crystalline Solids, 220, 139-146.

Mymrin, V., Praxedes, P. B., Alekseev, K., Avanci, M. A., Rolim, P. H., Povaluk, A. E., & Catai, R. E. (2019). Manufacturing of sustainable ceramics with improved mechanical properties from hazardous car paint waste to prevent environment pollution. The International Journal of Advanced Manufacturing Technology, 105(5-6), 2357-2367.

Mysen, B.O., & Richet, P. (2018). Silicate Glasses and Melts, Elsevier, Amsterdam.

Nandi, V. S., Raupp-Pereira, F., Montedo, O. R. K., & Oliveira, A. P. N. (2015). The use of ceramic sludge and recycled glass to obtain engobes for manufacturing ceramic tiles. Journal of Cleaner Production, 86, 461-470.

Ohashi, H., Osawa, T., & Sato, A. (1994). $NaVSi_2O_6$. Acta Crystallographica C, 50, 1652-1655.

O'Neill, H.S.C. & Dollase, W.A. (1994). Crystal structures and cation distributions in simple spinels from powder XRD structural refinements: $MgCr_2O_4$, $ZnCr_2O_4$, Fe_3O_4 and the temperature dependence of the cation distribution in $ZnAl_2O_4$. Physics and Chemistry of Minerals, 20, 541-555.

Ouahabi, M. E., Daoudi, L., Hatert, F., & Fagel, N. (2015). Modified mineral phases during clay ceramic firing. Clays and Clay Minerals, 63(5), 404-413.

Palmonari, C., & Timellini, G. (1982). Pollutant emission factors for the ceramic floor and wall tile industry. Journal of the Air Pollution Control Association, 32(10), 1095-1100.

Pan, D. A., Li, L. J., Yang, J., Bu, J. B., Guo, B., Liu, B., ... & Volinsky, A. A. (2015). Production of glass–ceramics from heavy metal gypsum and pickling sludge. International journal of environmental science and technology, 12(9), 3047-3052.

Pérez-Villarejo, L., Martínez-Martínez, S., Carrasco-Hurtado, B., Eliche-Quesada, D., Ureña-Nieto, C., & Sánchez-Soto, P. J. (2015). Valorization and inertización of galvanic sludge waste in clay bricks. Applied Clay Science, 105, 89-99.

Pinheiro, B. C. A., & Holanda, J. N. F. (2013). Reuse of solid petroleum waste in the manufacture of porcelain stoneware tile. Journal of Environmental management, 118, 205-210.

Ponsot, I., & Bernardo, E. (2013). Self glazed glass ceramic foams from metallurgical slag and recycled glass. Journal of cleaner production, 59, 245-250.

Ponsot, I., Bernardo, E., Bontempi, E., Depero, L., Detsch, R., Chinnam, R. K., & Boccaccini, A. R. (2015). Recycling of pre-stabilized municipal waste incinerator fly ash and soda-lime glass into sintered glass-ceramics. Journal of Cleaner Production, 89, 224-230.

Quijorna, N., Coz, A., Andres, A., & Cheeseman, C. (2012). Recycling of Waelz slag and waste foundry sand in red clay bricks. Resources, Conservation and Recycling, 65, 1-10.

Quijorna, N., Miguel, G. S., & Andrés, A. (2011). Incorporation of Waelz slag into commercial ceramic bricks: a practical example of industrial ecology. Industrial & Engineering Chemistry Research, 50(9), 5806-5814.

Raimondo, M., Zanelli, C., Matteucci, F., Guarini, G., Dondi, M., & Labrincha, J. A. (2007). Effect of waste glass (TV/PC cathodic tube and screen) on technological properties and sintering behaviour of porcelain stoneware tiles. Ceramics International, 33(4), 615-623.

Rajarathnam, U., Athalye, V., Ragavan, S., Maithel, S., Lalchandani, D., Kumar, S., Baum, E., Weyant, C. & Bond, T. (2014). Assessment of air pollutant emissions from brick kilns. Atmospheric Environment, 98, 549-553.

Rambaldi, E., Esposito, L., Andreola, F., Barbieri, L., Lancellotti, I., & Vassura, I. (2010). The recycling of MSWI bottom ash in silicate based ceramic. Ceramics International, 36(8), 2469-2476.

Ramos, A., Levelut, C., & Petiau, J. (1992). Local environment of selenium in silicate glasses. Journal of non-crystalline solids, 151, 13-22.

Raudsepp, M., Hawthorne, F.C., & Turnock, A.C. (1990). Crystal chemistry of synthetic pyroxenes on the join $CaNiSi_2O_6$-$CaMgSi_2O_6$ (diopside): A Rietveld refinement study. American Mineralogist, 75, 1274-1281.

Redhammer, G.J. & Roth, G. (2005). A comparison of the clinopyroxene compounds $CaZnSi_2O_6$ and $CaZnGe_2O_6$. Acta Crystallographica C, 61, i20-i22.

Redhammer, G.J., Tippelt, G., Merz, M., Roth, G., Treutmann, W., & Amthauer, G. (2005). Structure of the clinopyroxene-type compound $CaCuGe_2O_6$ between 15 and 800 K. Acta Crystallographica B, 61, 367-380.

Robinson, K., Gibbs, G.V., & Ribbe, P.H. (1971). Quadratic elongation: a quantitative measure of distortion in coordination polyhedra. Science, 172, 567-570.

Rocquefelte, X., Clabau, F., Paris, M., Deniard, P., Le Mercier, T., Jobic, S., & Whangbo, M.-H. (2007). Resolving the aluminum ordering in aluminosilicates by a combined experimental/theoretical study of [27]Al electric field gradients. Inorganic Chemistry, 46, 5456-5458.

Rüdorff, W. & Reuter, B. (1947). Die Struktur der Magnesium- und Zink- Vanadinspinelle. Beitrag zur Struktur der Spinelle. Zeitschrift für anorganische Chemie, 253, 194-208.

Saba, D., Manouchehri, N., Besançon, S., El Samad, O., Khozam, R.B., Kassir, L.N., Kassouf, A., Chebib, H., Ouaini, N., Cambier, P. (2019). Bioaccessibility of lead in Dittrichia viscosa plants and risk assessment of

human exposure around a fertilizer industry in Lebanon. Journal of Environmental Management, 250, 109537.

Schabbach, L. M., Andreola, F., Barbieri, L., Lancellotti, I., Karamanova, E., Ranguelov, B., & Karamanov, A. (2012). Post-treated incinerator bottom ash as alternative raw material for ceramic manufacturing. Journal of the European Ceramic Society, 32(11), 2843-2852.

Shafer, M.W. (1962). Preparation and properties of ferrospinels containing Ni^{3+}. Journal of Applied Physics 33, 1210-1211.

Sharifikolouei, E., Baino, F., Galletti, C., Fino, D., & Ferraris, M. (2020). Adsorption of Pb and Cd in rice husk and their immobilization in porous glass-ceramic structures. International Journal of Applied Ceramic Technology, 17(1), 105-112.

Shimizu, M., Kimata, M., & Iida, I. (1995). Crystal structure of $Ba_2MgSi_2O_7$ melilite: the longest tetrahedral Mg-O distance. Neues Jahrbuch fuer Mineralogie. Monatshefte, 39-47.

Sinha, A.P.B., Sanjana, N.R., & Biswas, A.B. (1957). On the structure of some manganites. Acta Crystallographica, 10, 439-440.

Smedskjaer, M. M., Youngman, R. E., & Mauro, J. C. (2013). Impact of ZnO on the structure and properties of sodium aluminosilicate glasses: Comparison with alkaline earth oxides. Journal of non-crystalline solids, 381, 58-64.

Sobiecka, E., Kołaciński, Z., Rincón, J. M., & Olejnik, T. P. (2019). Coloured sintered glass-ceramics from hospital incineration fly ash. Materials Letters, 252, 35-37.

Tan, W. F., Wang, L. A., Huang, C., Liu, Y. Y., Green, J. E., Newport, D., & Green, T. (2012). Utilization of municipal solid waste incineration fly ash in lightweight aggregates. Journal of Central South University, 19(3), 835-841.

Tang, Y., Wu, P., Shih, K., & Liao, C. (2019). Industrial sludge for ceramic products and its benefit for metal stabilization. In Industrial and Municipal Sludge (pp. 253-293). Butterworth-Heinemann.

Teo, P. T., Anasyida, A. S., Basu, P., & Nurulakmal, M. S. (2014). Recycling of Malaysia's electric arc furnace (EAF) slag waste into heavy-duty green ceramic tile. Waste management, 34(12), 2697-2708.

Terrones-Saeta, J. M., Suárez-Macías, J., Iglesias-Godino, F. J., & Corpas-Iglesias, F. A. (2020). Study of the Incorporation of Biomass Bottom Ashes in Ceramic Materials for the Manufacture of Bricks and Evaluation of Their Leachates. Materials, 13(9), 2099.

Thompson, L. M., & Stebbins, J. F. (2012). Non-stoichiometric non-bridging oxygens and five-coordinated aluminum in alkaline earth aluminosilicate glasses: Effect of modifier cation size. Journal of non-crystalline solids, 358, 1783-1789.

Tiwari, M.K., Bajpai, S., Dewangan, U.K, Tamrakar, R.K. (2015). Suitability of leaching test methods for fly ash and slag: A review. Journal of Radiation Research and Applied Sciences, 8, 523-537.

USEPA, United States Environmental Protection Agency (1986). Guidelines for the health risk assessment of chemical mixtures. Fed. Regist. 51, 34014–34025.

Vichaphund, S., Thavorniti, P., & Jiemsirilers, S. (2010). Properties of ceramic produced from clay and MSW incineration bottom ash mixtures. Science & Technology Asia, 89-93.

Vieira, C. M. F., Morais, A. S. C., Monteiro, S. N., & Delaqua, G. C. G. (2016). Teste industrial de cerâmica vermelha incorporada com resíduo de vidro de lâmpada fluorescente. Cerâmica, 62, 376-385.

Viswanathan, K., & Brandt, K. (1980). The crystal structure of a ternary (Ba, K, Na)-feldspar and its significance. American Mineralogist, 65, 472-476.

Wang, K. S., Chiang, K. Y., & Chu, W. T. (1997). Fate and partitioning of heavy metals affected by organic chloride content during a simulated municipal solid waste incineration process. Journal of Environmental Science & Health Part A, 32(7), 1877-1893.

Wang, K. S., Chiang, K. Y., Lin, S. M., Tsai, C. C., & Sun, C. J. (1999). Effects of chlorides on emissions of toxic compounds in waste incineration: study on partitioning characteristics of heavy metal. Chemosphere, 38(8), 1833-1849.

Yamanaka, T. (1986). Crystal structures of Ni_2SiO_4 and Fe_2SiO_4 as a function of temperature and heating duration. Physics and Chemistry of Minerals, 13, 227-232.

Yang, C.M., Chien, M.Y., Chao, P.C., Huang, C.M., & Chen, C.H. (2021). Investigation of toxic heavy metals content and estimation of potential health risks in Chinese herbal medicine. Journal of Hazardous Materials 412, 125-142.

Yasuhara, A., Katami, T., Okuda, T., Ohno, N., & Shibamoto, T. (2001). Formation of dioxins during the combustion of newspapers in the presence of sodium chloride and poly (vinyl chloride). Environmental science & technology, 35(7), 1373-1378.

Yin, K., Dou, X., Ren, F., Chan, W.P., Chang, V.W.P. (2018). Statistical comparison of leaching behavior of incineration bottom ash using seawater and deionized water: Significant findings based on several leaching methods. Journal of Hazardous Materials 344, 635–648.

Yoshida, S., Sudo, T., Kato, M., Sugawara, T., Matsuoka, J., Miura, Y., & Kii, Y. (2010). Effects of composition on redox behaviors of antimony or arsenic ion in silicate melts by differential pulse voltammetry. Journal of non-crystalline solids, 356, 2842-2849.

Yousaf, B., Liu, G., Abbas, Q., Wang, R., Imtiaz, M., & Rehman, M.Z. (2017). Investigating the uptake and acquisition of potentially toxic elements in plants and health risks associated with the addition of fresh biowaste amendments to industrially contaminated soil. Land Degradation & Development, 28, 8, 2596-2607.

Zanelli, C., Conte, S., Molinari, C., Soldati, R., & Dondi, M. (2021). Waste recycling in ceramic tiles: a technological outlook. Resources, Conservation and Recycling, 168, 105289.

Zanelli, C., Raimondo, M., Guarini, G., & Dondi, M. (2011). The vitreous phase of porcelain stoneware: composition, evolution during sintering and physical properties. Journal of Non-Crystalline Solids, 357, 3251-3260.

Zhang, J., Liu, B., & Zhang, S. (2021). A review of glass ceramic foams prepared from solid wastes: Processing, heavy-metal solidification and volatilization, applications. Science of The Total Environment, 146727.

Zhang, X., Ma, G., Jin, Y., & Cheng, P. (2014). Preparation of ceramic tiles with black pigments using stainless steel plant dust as a raw material. Ceramics International, 40(7), 9693-9700.

Zhao, S., Wen, Q., Zhang, X., Liu, B., & Zhang, S. (2021). Migration, transformation and solidification/stabilization mechanisms of heavy metals in glass-ceramics made from MSWI fly ash and pickling sludge. Ceramics International. (*in press*, DOI: 10.1016/j.ceramint.2021.04.172).

Zhou, J., Li, T., Zhang, Q., Wang, Y., & Shu, Z. (2013). Direct-utilization of sewage sludge to prepare split tiles. Ceramics International, 39(8), 9179-9186.

Zhu, H. M., Jiang, X. G., Yan, J. H., Chi, Y., & Cen, K. F. (2008). TG-FTIR analysis of PVC thermal degradation and HCl removal. Journal of analytical and applied pyrolysis, 82(1), 1-9.

Table 1. HE leaching: examples of acceptable limits (ξ_{limit}, in mg·L^{-1}) established for inert materials.

HE	EU (Dir. 1999/31/EC)		USA (EPA TCLP 1311-1)	CHINA	BRAZIL
	EN 12457-1 (2 L/kg)	EN 12457-2 (10 L/kg)		(GB 5085.3 2007)	NBR 10005
As	0.1	0.5	5.0	5.0	1.0
Ba	7.0	20.0	100.0	100.0	70.0
Cd	0.03	0.04	1.0	1.0	0.5
Cr$_{tot}$	0.2	0.5	5.0	15.0	5.0
Cu	0.9	2.0		100.0	
Hg	0.003	0.01	0.2	0.1	0.1
Mo	0.3	0.5			
Ni	0.2	0.4		5.0	
Pb	0.2	0.5	5.0	5.0	1.0
Sb	0.02	0.06			
Se	0.06	0.1	1.0	1.0	1.0
Zn	2.0	4.0		100.0	

Table 2. Literature case studies of HE inertisation for the waste incorporation into silicate ceramics: product types, waste sources, firing conditions, body types, leaching tests, and investigated HEs (numbers of available datasets).

Reference	Ceramic type	Waste source	Firing Temperature (°C)	Body type	Leaching test	Hazardous element										
						As	Ba	Cd	Cr	Cu	Mo	Ni	Pb	Se	Sb	Zn
Alonso-Santurde et al., 2008	B	harbour sediment	1125–1150	I	1-2	4	4	4		4						

46

Reference	Type	Waste	Temp	Phase	C1	C2	C3	C4	C5	C6	C7	C8	C9	C10	C11	C12
Alonso-Santurde et al., 2010	B	foundry sand	1020	III	2	1			1			1				
Alonso-Santurde et al., 2011	B	foundry sand	850	III	1-2	2	2		2	2		2	2		2	2
Andreola et al., 2019	T	MSWI bottom ash	1190–1210	I	2			2		2		2	2			2
Bantsis et al., 2011	T	electric arc furnace slag	1000	II	2	1							1			1
Bernardo et al., 2006	G	panel glass	880	II	5		2						2		2	
Bernardo et al., 2010	G	MSWI bottom ash	950	II	3				1							
Contreras et al., 2014	T	tionite	1150	I	3	1	1		1				1			1
Fernandez-P. et al., 2011	B	biomass gasification fly ash	1000–1075	II	3	3	3		3							3
Garcia-Valles et al., 2007	G	sewage + galvanic sludges	1100	II	6				1	1		1				1
Haiying et al., 2011	B	MSWI fly ash	950	II	4				1	1		1	1			1
Liu et al., 2019	T	red mud + insulator	1140	I	3	1		1	1	1		1				1
Martinez-Garcia et al., 2012	B	wastewater treatment sludge	950	II	3	6		6	6	6		6	6	6		6
Nandi et al., 2015	T	ceramic sludge + glass	1175	I	7		1					1				
Pinheiro et al., 2013	T	solid petroleum waste	1240	I	7		1									
Ponsot et	G	fly ash +	1050	II	2	1		1	1	1	1	1				1

Reference	Product	Waste material	Temp (°C)	Body									
al., 2015		soda-lime glass											
Quijorna et al., 2011	B	Waelz slag	850–930	II-III	1-2	8	8	8	8	8	8	8	8
Rambaldi et al., 2010	T	MSWI bottom ash	1120–1160	I	2					3		3	3
Schabbach et al., 2012	T	MSWI bottom ash	1190–1210	I	2					2		2	2
Tan et al., 2012	L	MSWI bottom ash	1130	I	4								1
Tang et al., 2019	G	chromite and galvanic sludges	900–1100	II	3				1	1			
Teo et al., 2014	T	electric arc furnace slag	1150	I	1		2	2	2			2	2
Unpublished data	T	ceramic sludge + glass	1180	I	1	1							
Vichapund et al., 2010	T	MSWI fly ash	1125	I	3								1
Zhang et al., 2014	T	stainless steel dust	1200	I	4	1			1	1		1	1
Zhou et al., 2013	T	sewage sludge	1210	I	3	1			1				

Ceramic product: B, clay bricks; G, glass-ceramics; L, lightweight aggregates; T, wall and floor tiles. Body type: largely vitrified (I), largely recrystallised (II), and largely unreacted (III). Leaching test: EN 12457-1 (1), EN 12457-2 (2), EPA TCLP 1311-1 (3), GB 5085.3 2007 (4), ENV 12506 (5), DIN 38414 S4 (6), NBR 10005 (7).

Table 3. HE allocation in aluminosilicate melts and glasses.

Elem.	Valence state	Oxygen coordination	Metal-oxygen distance (Å)	Complexes or oxyanions	Notes	References
Sb	Sb^{3+} predominant	Sb^{3+} [3]	Sb^{3+}–O 1.938	[:$Sb^{3+}O_3$] likely in	Sb^{5+} increasing with f_{O_2}, CaO and glass basicity	Mee et al. 2010
	Sb^{5+} minor	Sb^{5+} [6]	Sb^{5+}–O 1.964	4[:$Sb^{3+}O_3$] rings		Miller et al. 2019
As	As^{3+} predominant	As^{3+} [3]	As^{3+}–O 1.78	[:$As^{3+}O_3$]	As^{5+} increasing with f_{O_2} and glass basicity charge compensator of	Yoshida et al. 2010

Element	Species	Coordination	Bond distance	Structural unit	Notes	Reference
					Al^{3+} in tetrahedral coordination	
	As^{5+} minor	As^{5+} [4]				Maciag and Brenan 2020
Ba	Ba^{2+}	Ba^{2+} [12]	Ba^{2+}–O 2.75-3.5	$[Al^{3+}O_4]$–Ba^{2+}–$[Al^{3+}O_4]$		Djordjevic et al. 2001
						Thompson and Stebbins 2012
Cr	Cr^{3+} predominant	Cr^{3+} [6]	Cr^{3+}–O 1.96	Cr^{3+}–Cr^{3+} dimers	Cr^{6+} increasing with fo_2 and glass basicity. Cr^{4+} prevailing with glass modifiers >60%	Murata et al. 1997
	Cr^{4+} minor	Cr^{4+} [4]	Cr^{6+}–O 1.72	dominant for Cr_2O_3>0.25%		Choi et al. 2000
	Cr^{6+} minor	Cr^{6+} [4]		$[Cr^{6+}O_4]^{2-}$		Colson et al. 2000
Cu	Cu^+ predominant	Cu^+ [2]	Cu^+–O 1.84 [2]		Cu^{2+} increasing with fo_2 and glass basicity. Coordination number grows with Cu^+ %	Kamiya et al. 1992
	Cu^{2+} minor	Cu^+ [3] minor	Cu^+–O 1.88 [3]			Lee et al. 2000
		Cu^+ [4] minor	Cu^+–O 1.91 [4]			Holzheid and Lodders 2001
Pb	Pb^{2+}	Pb^{2+} [3]	Pb^{2+}–O [3] 2.24		PbO_3 and PbO_4 pyramidal	Méar et al. 2007
		Pb^{2+} [4] minor			units in lead silicate glasses	Kacem et al. 2017
Mo	Mo^{6+} predominant	Mo^{6+} [4]	Mo^{6+}–O 1.75-1.78	$[Mo^{6+}O_4]^{2-}$	Mo oxyanions are not connected with the glass tetrahedral network	Calas et al. 2003
	Mo^{4+} minor	Mo^{4+} [6]	Mo^{4+}–O 2.01-2.02	$[Mo^{4+}O_6]^{6-}$ molybdenyl $Mo^{4+}O^{2+}$		Farges et al. 2006
						McKeown et al. 2017
Ni	Ni^{2+}	Ni^{2+} [4]	Ni^{2+}–O 1.95 [4]		Ni^{2+} [4] stabilised by K	Galoisy and Calas 1993
		Ni^{2+} [5] minor	Ni^{2+}–O 2.00 [5]		Ni^{2+} [5] by Na, Ca, Mg	Kado et al. 2020
Se	Se^{6+}	Se^{6+} [3]	Se^{6+}–O 1.69 Å		fully inserted in the glass network but in Zn glasses	Ramos et al. 1992

49

V	V^{5+} predominant	V^{5+} [4]	V^{5+}–O 1.69-1.70	[V^{5+}O$_4$]$^{3-}$	V^{3+} is scarce	McKeown et al. 2002
	V^{4+} minor	V^{4+} [5]	V^{4+}–O 1.90			Mallmann and O'Neill 2009
Zn	Zn^{2+}	Zn^{2+} [4]	Zn^{2+}–O 1.95-1.96		glass network former	Calas et al. 2002
						Smedskjaer et al. 2013

Highlights

- Introduction of wastes in silicate ceramics in the perspective of circular economy
- Degree of inertization efficiency of ceramic process for nine hazardous elements
- Incorporation into ceramic products in both crystalline or vitreous phases
- High efficiency of ceramic process in different bodies and firing conditions
- Need to design a specific inertization strategy for Mo and As